2015

Determining the Molecular Mechanism Modulating Interactions Between Cardiac Potassium Channel α-Subunit Proteins hERG and KvLQT1

Yeon Joo Lee
ylee8@wellesley.edu

Determining the Molecular Mechanism Modulating Interactions Between Cardiac Potassium Channel α-Subunit Proteins hERG and KvLQT1

Yeon Joo Lee

Advisor: Louise E. O. Darling

Submitted in Partial Fulfillment of the Prerequisite for Honors
in the Neuroscience Program

Wellesley College
April 2015

Acknowledgements

I would like to thank the following people who made the writing of this thesis possible:

My amazing advisor, Louise Darling, for all of her support and wisdom throughout this process. Thank you for helping me grow and learn as a critical thinker and scientist for the past two and a half years;

The other members of the Darling lab, including Estelle Kim ’15, for collaborating with me for the past year as we both worked to answer similar biological questions through different methods and approaches, and Amanda Papakyrikos ’14 and Medeea Popescu ’17, for creating the V822M hERG mutant construct that I utilized for many of my experiments in this thesis;

My thesis committee members Marc Tetel and John Cameron for providing me with constructive advice and sharing ideas to help me make my thesis the best that it could be;

The Committee on Curriculum and Academic Policy for believing in the integrity and value of my research and granting me the Jerome A. Schiff Fellowship, as well as the Jerome A. Schiff Fellowship for helping to fund my work;

The Dean’s Office and the Neuroscience Program for providing me with the opportunity to carry out this research project.

Table of Contents

Abbreviations

hERG	Human ether-a-go-go protein; α-subunit of hERG protein complex
KvLQT1	α-subunit of KvLQT1 protein complex
hERG (KCNH2)	Gene encoding α-subunit hERG
KCNE1	Gene encoding α-subunit KvLQT1
APD	Action potential duration
MiRP1	MinK-related protein 1; β-subunit of hERG protein complex
minK	β-subunit of KvLQT1 protein complex
I_{Kr}	Rapid-delayed rectifying potassium current through hERG channel
I_{Ks}	Slow-delayed rectifying potassium current through KvLQT1 channel
LQTS	Long QT Syndrome
CNBhD	Cyclic Nucleotide Binding homology Domain
CHOs	Chinese Hamster Ovary Cells
HEKs	Human Embryonic Kidney Cells
wt	Wild-type
pCPT-cAMP	8-(4-Chlorophenylthio)adenosine 3',5'-cyclic monophosphate sodium salt
IBMX	3-Isobutyl-1-methlxanthine
PKA	Protein Kinase A
apFRET	Acceptor photobleaching fluorescence resonance energy transfer
E_f	FRET efficiency in experimental regions
C_f	Control for false-positive FRET efficiency

Abstract

KvLQT1 and hERG are the voltage-gated K^+ channel α-subunits of the cardiac repolarizing currents I_{Ks} and I_{Kr}, respectively. These currents function to maintain proper action potential durations in cardiomyocytes to ultimately promote a normal heartbeat. Mutations in *KCNQ1* or *hERG* can lead to a loss of proper function in these currents, resulting in arrhythmias. Previous research in transgenic model organisms demonstrated that interactions between pore mutants of KvLQT1 and hERG exist, resulting in mutual downregulation of their respective currents. In addition, direct protein-protein interactions between wild-type hERG and KvLQT1, and more specifically between the COOH-termini of the two proteins, have been established. These interactions have been shown to result in downregulation of the repolarizing currents in heterologous cells. We hypothesize that hERG-KvLQT1 interactions are abrogated through direct binding of cAMP to the cyclic nucleotide binding homology domain (CNBhD) in the C-terminus of hERG, rather than by downstream, PKA-mediated effects. In order to delineate the molecular mechanism underlying these interactions, quantitative FRET analyses were performed on human embryonic kidney (HEK) cells co-expressing either wild-type hERG and KvLQT1, or the V822M hERG mutant and wild-type KvLQT1. Intracellular cAMP levels were elevated through membrane-permeable cAMP analogs and IBMX. Mean FRET efficiency of wild-type hERG and KvLQT1 was significantly reduced in the presence of elevated intracellular cAMP levels, while the mean FRET efficiency of mutant hERG and KvLQT1 was not significantly affected. The effect of elevated cAMP levels on the interactions between wild-type hERG and KvLQT1 compared to those between mutant hERG and KvLQT1 still remains inconclusive. In light of current progress in the field, however, the potential for cAMP-dependent PKA phosphorylation of hERG and/or KvLQT1 will also be explored. This work potentially furthers our understanding of the physiological regulation of hERG-KvLQT1 interactions and its implications on cardiac arrhythmias in both healthy and diseased states, as well as characterizes novel interactions between two distinct potassium channel families.

Introduction

The heart acts as a mechanical pump responsible for delivering oxygenated blood to all of the cells of the body. The mechanical function of this organ is regulated by synchronous electrical activity of the muscle cells of the heart, referred to as cardiomyocytes. In humans, the cardiac action potential is dependent on the influx and efflux of various ions and can be divided into five distinct phases (Sanguinetti and Tristani-Firouzi, 2006). Depolarization occurs during phase 0 of the action potential and is a result of a rapid influx of sodium, referred to as the sodium current, or I_{Na}, while repolarization is mainly the result of the efflux of potassium ions (Grant, 2009). In the cardiomyocyte, repolarization is a much slower process (Figure 1), occurring over the course of phases 1, characterized by a rapid, short depolarization, 2, characterized by a plateau of repolarization, 3, characterized by a more prominent depolarization of the membrane potential, and 4, characterized by complete repolarization and representative of the resting membrane potential, which would continually persist without the triggered influx of sodium to effectively restart the cycle (Sanguinetti and Tristani-Firouzi, 2006). The collective activity of multiple cardiomyocytes results in activity at the organ level, namely the heartbeat (Figure 1).

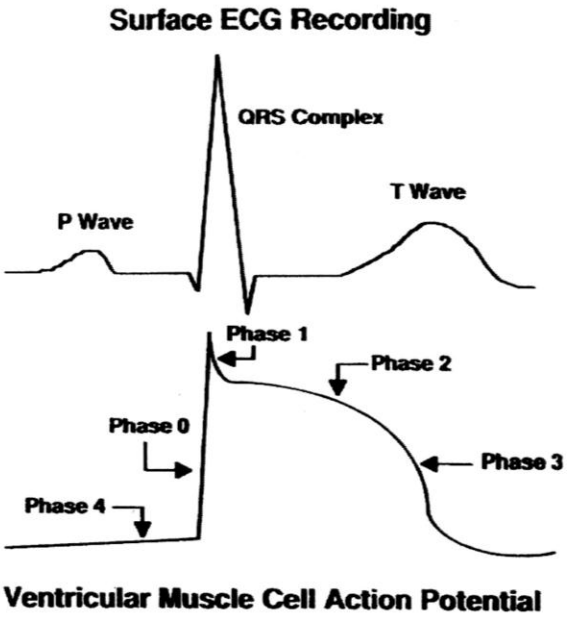

Figure 1. The top figure depicts a normal surface ECG recording, and the figure below represents the corresponding action potential for a normal cardiomyocyte. The P wave represents atrial depolarization, the QRS complex represents atrial repolarization and simultaneous ventricular depolarization, and the T wave represents ventricular repolarization. The action potential demonstrates the various phases that correspond to each portion of the ECG recording.
Credit: http://intranet.tdmu.edu.ua/data/kafedra/internal/normal_phiz/classes_stud/en/pharm/prov_pharm/1%20course/4%20Cycle%20Physiology%20of%20blood%20circulation/01%20Physiological%20properties%20of%20heart_ECG_Pumping%20work%20of%20the%20heart_Neuro-humeral%20regulation%20of%20the%20heart.htm

There are multiple kinds of potassium currents responsible for repolarization, while only one kind of sodium current exists for depolarization (Grant, 2009). There are then different kinds of potassium channels responsible for the different potassium currents. Specifically, there are 7 different potassium currents that are regulated by 5 different potassium channels (Grant, 2007).

hERG and KvLQT1 are two voltage-gated potassium channel protein subunits located in the plasma membrane of cardiomyocytes. The currents they carry are responsible for repolarizing the cardiac action potential during phase 3 of the cardiac action potential, as well as during phase 2 to offset the Ca^{2+} current, resulting in the characteristic plateau (Vandenberg et al., 2012; Jespersen et al., 2005). These repolarizing currents are essential to maintain proper action potential durations (APD) in cardiomyocytes to ultimately promote a normal heartbeat (Beeler and Reuter, 1977). Loss

of proper function in these currents can result in arrhythmias and, if untreated, sudden cardiac arrest (Sanguinetti and Tristiani-Firouzi, 2006). There are multiple potassium channels involved in maintaining APD, believed to be involved in a compensatory mechanism, or "repolarization reserve", in the event that one channel loses or alters its function (Roden, 2008). Previous studies on transgenic model organisms of long QT syndrome (LQTS) demonstrated that the presence of mutant KvLQT1 resulted in the expected loss of I_{Ks}, as well as an unexpected, functional downregulation of I_{Kr}, and vice versa (Brunner et al., 2008). This functional, mutual downregulation of hERG and KvLQT1 suggests that these proteins are somehow interacting, or "communicating", with one another, which may have negative physiological consequences.

hERG (KCNH2)

hERG (human ether-a-go-go related gene), or *KCNH2*, is located on chromosome 7 and specifically encodes the pore-forming α-subunit protein of the hERG channel that is responsible for the I_{Kr} current (Vandenberg et al., 2012). hERG is 1159 amino acids long with a cyclic nucleotide binding homology domain (CNBhD) located in the COOH-terminus (Warmke and Ganetzky, 1994; Vandenberg et al., 2012). The α-subunit of this channel possesses 6 transmembrane regions (Vandenberg et al., 2012). Four, identical α-subunits come together to form the pore of the channel through which potassium ions flow (Vandenberg et al., 2012). As an ion channel complex, hERG also assembles with its β-subunit, MinK-related peptide 1 (MiRP1), which is encoded by the gene *KCNE2*, although it does not appear that the expression of MiRP1 is necessary for hERG function, that is, creating the I_{Kr} current similar to native or *ex vivo* cardiomyocytes (Gabbott et al.,

1999; Weerapura et al., 2002). A visual representation of hERG and MiRP1 in the cell membrane is presented in Figure 2.

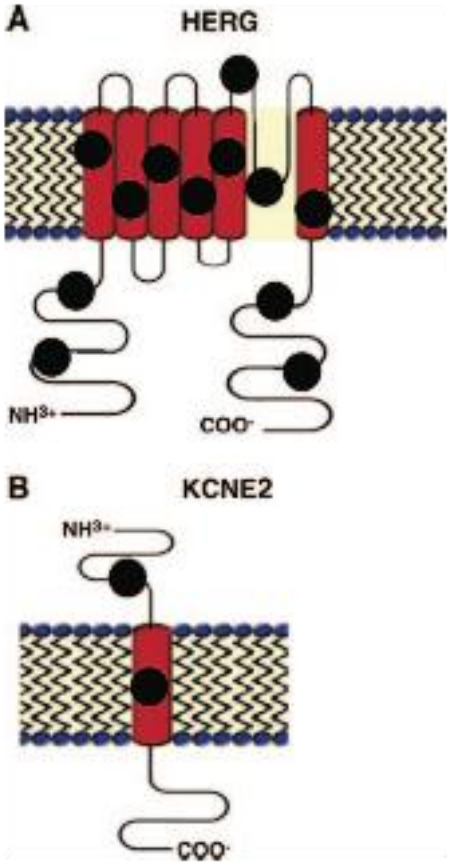

Figure 2. (A) represents the topology of the hERG α subunits that may assemble with MiRP1 (B) to form the I_{Kr} channel. The localization and function of MiRP1 are still relatively unknown and under investigation. The black dots represent the location of various identified mutations of hERG and MiRP1 associated with different forms of LQT syndrome. ***Clancy and Kass, 2005***

KCNQ1

KCNQ1 is located on chromosome 11 and encodes the α-subunit of the KvLQT1 channel that assembles with the *KCNE1* β-subunit (minK) and forms a channel complex constituting the delayed rectifier current I_{Ks} in cardiomyocytes (Barhanin et al., 1996; Sanguinetti et al., 1996; Jespersen et al., 2005). A single KvLQT1 subunit also possesses 6 transmembrane regions (Jespersen et al., 2005). The α-subunit is 676 amino acids in length, four of which come together to form the homotetrameric KvLQT1 channel pore

(Jespersen et al., 2005). β-subunit assembly with the α-subunits in this case is critical for proper I_{Ks} production (Barhanin et al., 1996; Sanguinetti et al., 1996). A visual representation of the topology of KvLQT1 and its β-subunit is presented in Figure 3.

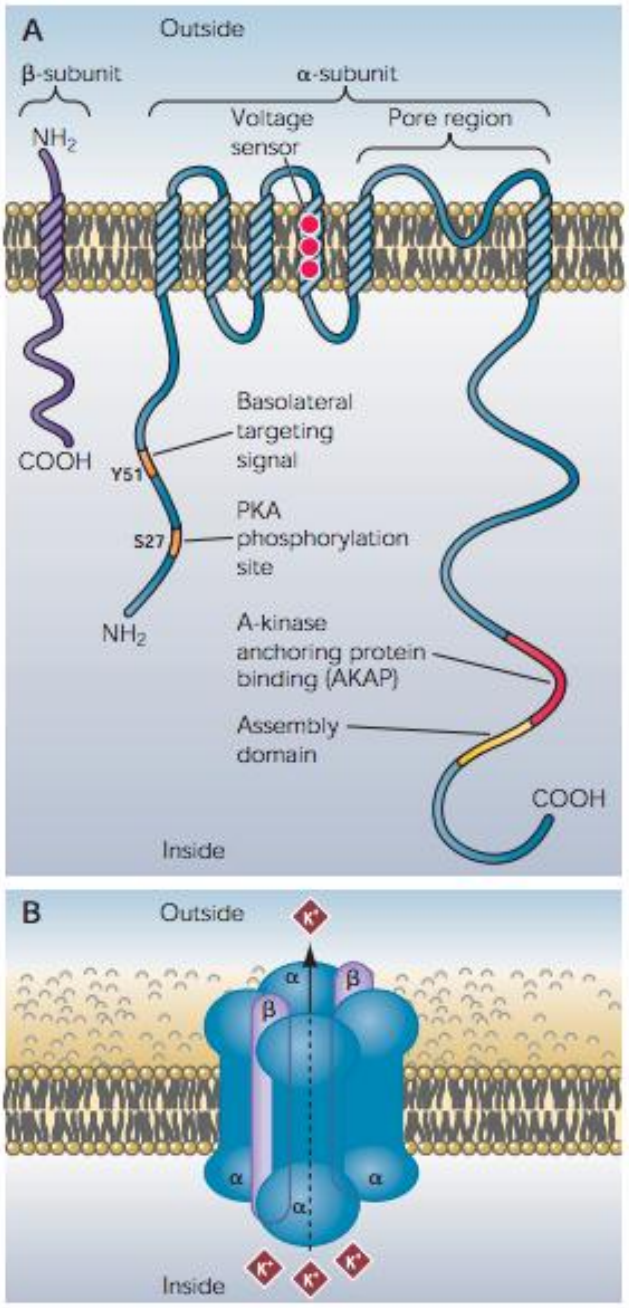

Figure 3. (A) represents the topology of the KvLQT1 and minK subunits forming the I_{Ks} potassium channel. Note the location of the minK subunit in relation to KvLQT1, this allows minK to interact with the ion channel portion of KvLQT1 and delay inactivation of the channel. (B) represents a three dimensional depiction of the KvLQT1-minK channel complex in the plasma membrane. ***Jespersen et al., 2005***

Motivation

The redundancy in the function of the repolarizing currents and the presence of different kinds of potassium channels suggest a potential evolutionary purpose for multiple repolarizing potassium channels proteins. This concept of a "repolarization reserve" has been characterized as a failsafe type of mechanism for maintenance of normal APD in the event that one potassium channel is blocked or impaired under normal physiological conditions (Biliczki et al., 2002). However, in the case that the current density of one of the channels is decreased as a result of genetic inheritance, such as in certain forms of LQTS, a cardiac condition in which the QT phase observed on an ECG (Figure 1) is prolonged, the "repolarization reserve" is essentially depleted because one channel is mutated, placing these patients at an increased risk for arrhythmia (Biliczki et al., 2002).

Brunner et al. (2008) reported two transgenic rabbit models of LQTS in which there was a dominant-negative overexpression of the pore mutants of KvLQT1, corresponding to LQT1, or pore mutants of hERG, corresponding to LQT2. Expression of these pore mutants resulted in the loss of I_{Ks} and I_{Kr} currents, respectively, as expected (Brunner et al., 2008). However, they also observed a significant downregulation of the complementary currents, I_{Kr} and I_{Ks}, respectively, without any evidence of decreased protein expression levels (Brunner et al., 2008). This physiological observation suggested the presence of dynamic hERG-KvLQT1 interactions (Brunner et al., 2008).

The results from Brunner et al. (2008) demonstrating the mutual, functional downregulation of I_{Ks} and I_{Kr} in the transgenic rabbit models of LQT syndrome prompted the assessment of interactions between hERG and KvLQT1 in heterologous cell lines by

Ren et al. (2010), due to the difficulty of culturing primary cardiomyocytes as well as the complexity in analyzing single currents in an excitable cell system. They found that transiently expressing pore mutant or wild-type (wt) KvLQT1 in Chinese Hamster Ovary cells (CHOs) stably expressing wt hERG both resulted in significant downregulation of I_{Kr} (Ren et al., 2010). They observed a similar downregulation of I_{Ks} when pore mutant or wt hERG was transiently expressed in CHOs stably expressing wt KvLQT1 (Ren et al., 2010). Furthermore, they found that (1) the deletion of the NH_2-terminus of KvLQT1 did not eliminate interactions, suggesting that the N-terminus of KvLQT1 is not necessary for these interactions, (2) co-immunoprecipitations demonstrated specific interactions between hERG and KvLQT1; and (3) surface plasmon resonance experiments demonstrated that the C-termimus of KvLQT1 interacts directly with C-terminus of hERG (Ren et al., 2010).

Additional studies have also demonstrated that hERG and KvLQT1 interact directly and specifically. Ehrlich et al. (2004) determined that hERG and KvLQT1 interact based on biophysical and biochemical evidence. They found that hERG current density doubled when hERG was co-expressed with KvLQT1, while membrane localization of hERG also increased when KvLQT1 was co-expressed (Ehrlich et al., 2004). Biliczki et al. (2009) demonstrated that expressing a trafficking-deficient KvLQT1 mutant failed to enhance membrane localization of hERG and reduced the I_{Kr} current that is normally observed in the presence of wt KvLQT1. These results suggest the potential role of such interactions and/or the disturbances in these interactions in attributing to the clinical phenotypes of congenital heart conditions (Biliczki et al., 2009).

Organ-Darling et al. (2013) went on to assess the nuances of the hERG-KvLQT1 interactions in human embryonic kidney (HEK) cells, another heterologous cell line useful as an *in vitro* model system, and in primary neonatal rabbit cardiomyocytes using acceptor photobleach fluorescence resonance energy transfer (apFRET) experiments, a quantitative method for measuring protein interactions in intact cells. Organ-Darling et al. (2013) were able to measure FRET efficiencies to demonstrate direct hERG-KvLQT1 interactions between the C-termini of the two proteins. Moreover, they demonstrated that increasing intracellular cAMP levels via acute treatment of hERG- and KvLQT1-expressing cells with two chemicals, IBMX, a phosphodiesterase inhibitor, and pCPT-cAMP, a permeable analogue of cAMP, together reduced these interactions. These results, in addition to the presence of a CNBhD in the portion of hERG that interacts with KvLQT1, suggested a direct role of the CNBhD in mediating these interactions (Warmke and Ganetzky, 1994; Organ-Darling et al., 2013). Therefore, this study provides the motivation for the focus of my thesis specifically addressing the role of the CNBhD and cAMP in mediating hERG-KvLQT1 interactions at the molecular level.

Cyclic adenosine 3',5'-monophosphate (cAMP) is a ubiquitous secondary messenger found in a wide range of cell types responsible for a diverse range of cellular signaling pathways and functions (Fimia and Sassone-Carsi, 2001). One of its functions is to activate the enzyme protein kinase A (PKA), which phosphorylates many kinds of proteins that are involved in a variety of pathways within the cell (Fimia and Sassone-Carsi, 2001). More specifically in cardiac physiology, cAMP levels increase as a result of epinephrine binding to its G-protein coupled receptor, the β-adrenergic receptor, resulting in the activation of adenylyl cyclase and the production of cAMP (Benovic et al., 1986).

The secondary messenger then goes onto activate PKA, which goes onto phosphorylate a host of other protein targets, one of which includes KvLQT1 (Benovic et al., 1986). The KvLQT1 phosphorylation pathway has been generally well-characterized. The I_{Ks} current increases in response to inputs from the sympathetic nervous system in order to increase heart rate and contractility, and to shorten the APD (Cheng et al., 2004). Marx et al. (2002) reported that cAMP-dependent PKA activity is responsible for phosphorylating KvLQT1 and its β-subunit minK (Marx et al., 2002). They also reported that elevating cAMP levels resulted in an increase in I_{Ks}, while the S27A substitution at a KCNQ1 phosphorylation site eliminated cAMP-dependent enhancement of the KCNQ1-KCNE1 current (Marx et al., 2002). The same pathway involving cAMP-dependent KvLQT1 phosphorylation at the N-terminus by PKA was elucidated by and expanded upon by other groups (Kurokawa et al., 2003; Nicholas et al., 2008)

Because cAMP is involved in many cellular processes, it would be a reasonable to speculate that downstream, PKA-mediated effects are responsible for modulating the direct interactions between hERG and KvLQT1 through hERG phosphorylation, and that the role of cAMP in this pathway is its general function of activating PKA (Cui et al., 2001). Indeed it appears that PKA does phosphorylate hERG downstream of adenylyl cyclase activity, thereby altering hERG channel electrophysiology (Cui et al., 2000; Kiehn, 2000). However, the presence of a CNBhD on the C-terminus of hERG suggests that cAMP plays a more direct role in the modulation of hERG-KvLQT1 interactions (Warmke and Ganetzsky, 1994; Cui et al. 2000).

A CNBD homology domain is present in various families of ion channels, including the ether-a-go-go (eag) family, of which hERG is a member, the

hyperpolarization-activated cyclic-nucleotide-modulated family, and the cyclic-nucleotide-gated family (Akhavan et al., 2005; Brelidze et al., 2009). Typically, its presence on channels suggests that these proteins are directly modulated by a cyclic nucleotide such as cAMP or cGMP (Akhavan et al., 2005). Previous studies have demonstrated that mutations or defects in the CNBhD of eag and KCNH channels have resulted in abnormal protein trafficking (Cui et al., 2001; Akhavan et al., 2005). Akhavan et al. demonstrated that the removal of the entire CNBhD on hERG prevented normal trafficking and surface expression, and thus function, of the hERG complex (Akhavan et al., 2005). Satler et al. (1996) identified a specific missense mutation in the CNBhD of hERG, in which the highly conserved valine at position 822 is replaced with a methionine, which appears to cause LQT2 by disrupting the function of the domain and thus causing an abnormal repolarizing current. The V822M mutation in hERG associated with LQT syndrome, along with the similarities between the CNBhD of hERG and other cyclic nucleotide gated channels, suggests that cAMP is involved in modulating hERG function and excitability (Bruggemann et al., 1993; Satler et al. 1996).

However, it should be noted that we refer to the CNBD on hERG as a "homology domain" due to contending views about the true ability of this domain to bind cAMP. Cui et al. (2000) suggest that cAMP mediates hERG function via two parallel pathways involving PKA downstream of cAMP and the direct binding of cAMP at the CNBhD. In order to test the role of PKA-mediated phosphorylation of hERG on hERG function, the group utilized the specific peptide inhibitor PKI (Cui et al., 2000). They also identified and mutagenized PKA phosphorylation sites on hERG to prevent phosphorylation from occurring (Cui et al., 2000). They saw that cAMP-dependent PKA phosphorylation of

hERG did not occur under these conditions (Cui et al., 2000). In order to test the direct role of the CNBhD in regulating hERG currents, binding assays of labeled cAMP to hERG were performed *in vitro* (Cui et al., 2000). Electrophysiology experiments were also performed to assess these effects on hERG function (Cui et al., 2000). Ultimately, the combinatory effects of cAMP-dependent PKA phosphorylation of hERG and direct binding of cAMP to hERG resulted in a decreased hERG current (Cui et al., 2000). Interestingly, however, Cui et al. (2000) also observed that in the presence of β-subunit proteins MiRP1 or minK, the stimulatory effects of direct cAMP binding on I_{Kr} was accentuated.

While groups, such as Thomas McDonald's group at Albert Einstein College of Medicine, which includes members from Cui et al. (2000), have claimed that cAMP directly binds to the CNBD on hERG, others have contended this view. Brelidze et al. (2009) reported that cAMP binds with very low affinity to the CNBhD of isolated hERG1 proteins, and that this binding does not affect hERG current, even at high concentrations of cAMP. Li et al. (2014) utilized NMR to demonstrate that cAMP does not directly bind to the CNBD on hERG. Others have determined the crystal structures of isolated CNBhDs of various KCNH channels, such as EAG and EAG-like channels (Brelidze et al., 2012; Marques-Carvalho et al., 2012). They have shown that these CNBhDs do not bind cyclic nucleotides and are instead occupied by short β-strands or COOH-terminus residues (Brelidze et al., 2012; Marques-Carvalho et al., 2012). Brelidze et al. (2012) have also shown that mutating these β-strands, preventing them from binding to the CNBhD, depolarized the voltage of activation, which suggests that KCNH2 channels are

"self-liganded". These studies shed light onto the possibility that the CNBhD may not actually play a direct role in hERG-KvLQT1 interactions.

The Darling lab is actively seeking to illuminate the cellular and molecular mechanisms of the direct interactions between hERG and KvLQT1 and to determine the functional consequences of such interactions. Initially, we hypothesized that the direct hERG-KvLQT1 interactions are modulated by direct binding of the ubiquitous intracellular signaling molecule cAMP at the CNBhD located in the COOH-terminus of hERG. The following experiments were performed in order to address this particular role of the CNBhD of hERG in mediating these interactions. However, do note that due to the current perspective of the field as described above, we understand that the PKA-mediated pathway is of biological significance to study in the future. Elucidating the underlying mechanisms regulating hERG-KvLQT1 interactions may help to understand the molecular origins of many types of arrhythmias and LQTS, as well as to aid in the development of their treatments.

Scientific Approach

The first aim of my thesis was to assess the role of intracellular cAMP levels in modulating hERG-KvLQT1 interactions at the molecular level. Again, the presence of direct interactions between hERG and KvLQT1 has been identified based on results from previous studies demonstrating the ability of KvLQT1 to rescue hERG protein trafficking to the cell membrane (Ehrlich et al., 2004), as well as other studies utilizing FRET and co-IP methodologies to show that hERG and KvLQT1 interact when co-expressed in *in vitro* model systems (Biliczki et al., 2009; Ren et al., 2010; Organ-Darling et al., 2013).

In order to address this question, acceptor photobleach FRET, or apFRET, experiments were performed in HEK cells expressing wt hERG and KvLQT1 tagged with fluorophores mCFP and mYFP, respectively. FRET, or Forster (fluorescence) resonance energy transfer, is a physical phenomenon that occurs between two light-sensitive molecules, which involves the radiation-less transfer of energy from a "donor" molecule to an "acceptor" molecule (Sun et al., 2013). Figure 4 provides a representation of the FRET phenomenon and how it is utilized in apFRET experiments. While the role of cAMP has been introduced previously by Organ-Darling et al. (2013), it was still of significant importance to validate the reproducibility of these results as a part of my project because ongoing apFRET experiments are performed on instrumentation and software different from those utilized in the Organ-Darling et al. study (2013).

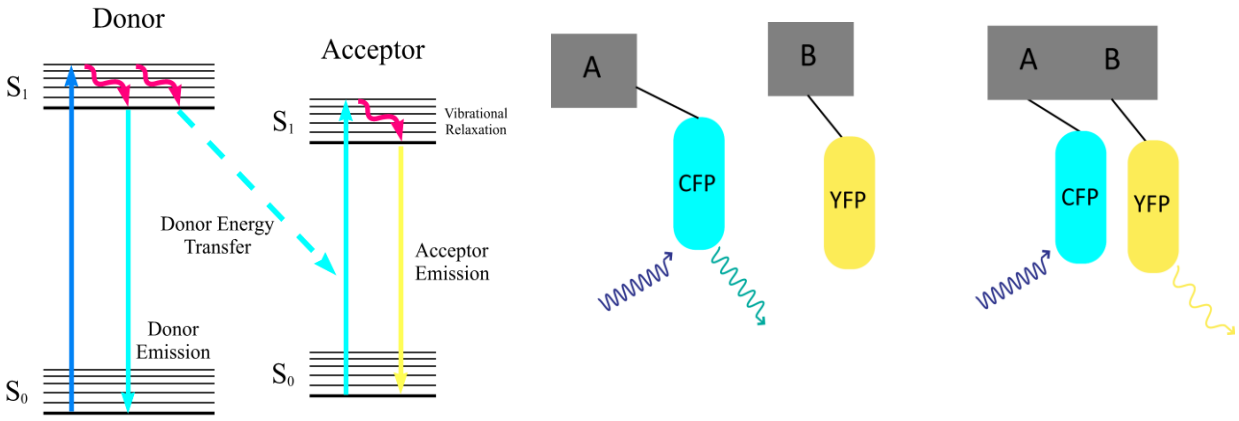

Figure 4. The diagram on the left demonstrates FRET, which is the radiation-less transfer of energy from a donor to an acceptor molecule, using fluorescence pairs. The laser excites electrons in the molecule to a higher energy level and transfers that energy to the neighboring molecule. These electrons then fall back to their original energy level, emitting light. The diagram on the right relates this principle to the use of fluorophores attached to proteins. When the two proteins are within 10nm of each other, a laser can excite one fluorophore and the energy will be transferred and emitted form the second fluorophore. The color change of the emission signals the energy transfer. The efficiency of this transfer can be quantified. **Figures created and adapted by L.E. Organ-Darling**

Prior to performing apFRET experiments, it was necessary to optimize the parameters of the FRET AB Wizard on the Leica TCS SP5 II, such as the CFP and YFP transmission percentages and the spectral emission ranges for CFP and YFP, as previous experiments were performed on a Zeiss LSM 510 microscope (Organ-Darling et al., 2013).

My second aim was to determine the molecular mechanism responsible for modulating the hERG-KvLQT1 interactions. More specifically, my focus was to determine whether hERG-KvLQT1 interactions are regulated by direct binding of cAMP at the CNBhD of hERG. apFRET experiments were also utilized to address this aim. In this case, rather than co-expressing wt proteins in HEK cells, the naturally occurring LQT1 mutant of hERG, V822M, which occurs in the CNBhD and renders the binding domain functionless but retain normal biosynthesis and trafficking, as reported by Cui et al. (2001), was co-expressed with wt KvLQT1. Utilizing the CNBhD hERG mutant was a direct way of assessing the role of the CNBhD in modulating the dynamics of hERG-KvLQT1 interactions at the molecular level.

Methods and Materials

hERG Mutant Construct Creation

The hERG-V822M-mCFP construct was created by Medeea Popescu ’17 and Amanda Papakyrikos ’14 by site-directed mutagenesis using the QuikChange Lightning multi site-directed mutagenesis kit (Agilent Technologies). The “m” in mCFP stands for monomerized. It was necessary to monomerize the CFP fluorophore to ensure that only a single fluorophore was linked to each protein. These fluorophores can form non-obligate

dimers if not monomerized. This could potentially lead to false positives during FRET experiments because the fluorophores themselves could be directly interacting with each other.

Cell Culture and Transfection

Human embryonic kidney 293 (HEK) cells were cultured in EMEM media (ATCC, product number 30-2003) with 10% FBS and 1% pen-strep (Life Technologies, catalog number 15070) under standard conditions and incubated at 37°C. For imaging, HEK cells were plated 24 hours before transfection on coverslips in tissue-culture treated 6-well plates at a density of 50,000 cells/slip. HEK cells were transiently transfected following product literature using X-tremeGENE 9 (Roche) transfection reagent with a ratio of 2 μl X-tremeGENE:1 μg DNA. For wt protein samples, cells were transfected with hERG-mCFP (wt negative control), KCNQ1-CFP-YFP (wt positive control), or hERG-mCFP + KCNQ1-mYFP (wt FRET pair). For hERG mutant samples, cells were transfected with hERG-V822M-mCFP (mutant negative control), KCNQ1-CFP-YFP, or hERG-V822M-mCFP + KCNQ1-mYFP (mutant FRET pair). Co-transfections for FRET pairs used equal mounts (1 μg) for each plasmid. Transfected cells were allowed to grow for 48 hours before any experiments took place. The medium was replaced 24 hours post transfection.

48 hours after transfection, intracellular cAMP levels were elevated through the application of 500 μM of the soluble cAMP analogue pCPT-cAMP (stock solution in dH_2O) (Sigma-Aldrich, product number C3912) and 100 μM of the phosphodiesterase inhibitor IBMX (stock solution in dH_2O) (Sigma-Aldrich, product number I5879) in cell

media. Cells were incubated with pCPT-cAMP and IBMX at 37°C for 5 minutes. After treatment, the cells were rinsed once with PBS. Following the first rinse, cells were fixed with 4% paraformaldehyde for 15 minutes. After fixing, the cells were rinsed 3X with PBS. The coverslips were mounted onto slides with Prolong Gold Diamond antifade mountant without DAPI (Life Technologies, catalog number P36934) and left to sit for 30 minutes, after which the coverslips were sealed with clear nail polish. Throughout this entire procedure, the cells were covered with tinfoil to prevent the cells from being exposed to light.

Confocal Imaging and Acceptor Photobleach FRET

Acceptor Photobleach FRET (apFRET) experiments were performed on a Leica TCS SP5 II following the provided FRET AB Wizard program. The mCFP and mYFP fluorophores were excited with 458- and 514-nm lasers, respectively. The transmission percentages were held at 20% and 10% for the 458- and 514-nm laser lines, respectively. The spectral emission ranges for CFP and YFP were set to 470-510 nm and 580-650 nm, respectively. Eight-bit, 512 x 512 images of cells expressing the protein(s) were obtained with a 63X objective/1.40 oil UV at a zoom factor of 2 with a pinhole of 1 Airy units, corresponding to an image depth of 95.51 μm. For each cell, a circular region of interest (ROI) of 2.5 μm in diameter, representing the bleach ROI, was drawn in at the membrane of the cell, with approximately one half of the ROI on the cell and the other half in the background (Figure 5).

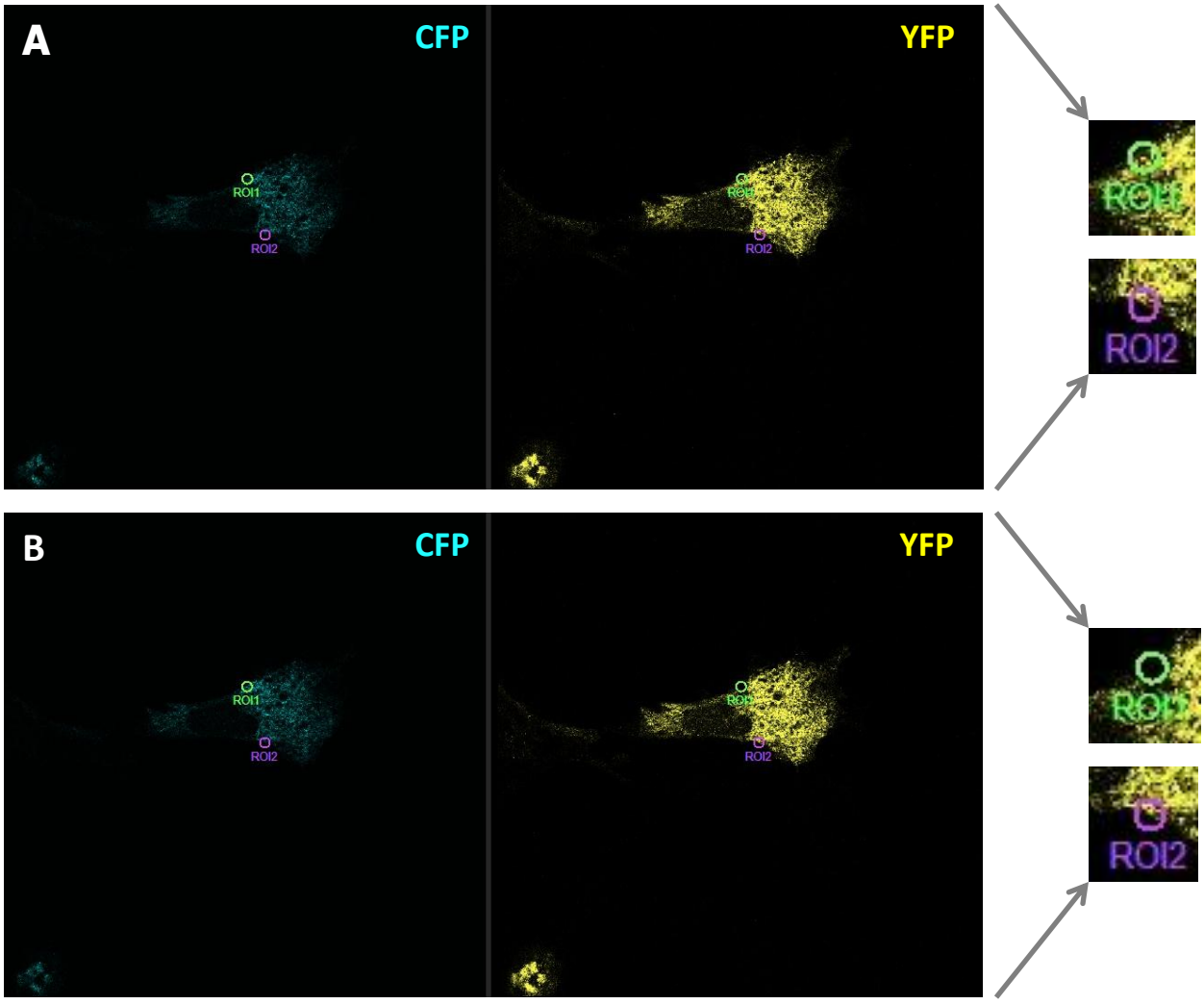

Bleach Region	
Donor Pre	26.46
Donor Post	38.6
Acceptor Pre	54.25
Acceptor Post	6.37
Bleach Depth	0.88
Efficiency	0.3146

Control Region	
Donor Pre	21.2
Donor Post	21.18
Acceptor Pre	45.69
Acceptor Post	48.27
Bleach Depth	0
Efficiency	0

Figure 5. ***A visual representation of the apFRET protocol on Leica FRET AB Wizard software.*** This representative experiment demonstrates direct interactions between CFP and YFP fluorescent proteins directly linked together and fused to the COOH-terminus of KvLQT1 (KCNQ1-CFP-YFP) expressed in Human Embryonic Kidney (HEK) cells. The region of interest (ROI) 1 of cell was bleached with 514 nm laser at 30% transmission for 5 seconds. ROI2 represents an unbleached, control region. (A) Representative images of cells expressing KvLQT1-CFP-YFP under FRET AB Wizard parameters pre-bleach. ROIs 1 and 2 are zoomed in. (B) Representative images of cells in (A) post-bleach. ROIs 1 and 2 are zoomed in. The tables below represent the pre and post intensity values of the donor and acceptor provided by the Wizard. Bleach depth and efficiency were calculated based on these intensity values. Images were taken with a 63X objective and a zoom of 2X and 1 Airy Unit on confocal microscope. *Note:* Images shown here have been contrast enhanced for better qualitative visualization in this thesis.

Photobleaching of the acceptor molecule (mYFP) was accomplished using the 514 laser line at 30% transmission for 5 rapid scans of the bleach ROI, requiring 5 s. The Leica FRET AB Wizard quantified the mean donor and acceptor intensity in the bleach region over time. The FRET efficiency (E_f) was calculated as E_f = (Ipostbleach-Iprebleach) x (100%/Ipostbleach), where I is the average mCFP (donor) intensity from the raw data in the bleach ROI for a given time point. FRET efficiencies below 0% were reported as 0 by the FRET AB Wizard, and therefore, these zero values were utilized as such in the data analyses. After running the apFRET experiment, it was necessary to go back to the original image and draw in another ROI of the same dimensions on the same cell in an area separate from the bleach region. This ROI acted as the control region, and the raw data was provided in a similar table as that of the bleach region (Fig. 5). Analogous equations used data from the control ROI to provide an internal, experimental control for false-positive FRET efficiencies (C_f) in each cell.

Statistical Analysis

A 3-way ANOVA without interactions was performed to analyze an effect of group-type (positive control, negative control, or FRET pair), treatment-type (pCPT-cAMP + IBMX treated or untreated), and mutant-type (wt or V822M hERG) across all samples to establish significance of group type, treatment type, and mutant type across all data points. A 2-factor ANOVA without interactions was also performed in order to determine the effect of treatment-type (pCPT-cAMP + IBMX treated or untreated) and mutant-type (wt or V822M hERG) across the FRET efficiencies of only the wt and mutant FRET pairs. *Post-hoc* student's t-tests were performed following ANOVAs as

necessary. ANOVA analyses were performed using *R* software. Significance was established at $p < 0.05$.

Results

Optimization of FRET AB Wizard Parameters

Prior to performing apFRET experiments, the parameters of the FRET AB Wizard on a Leica TCS SP5 II were optimized. It was necessary to determine an optimal transmission percentage, which is the amount of light that actually hits the sample, for each laser to ensure that neither the CFP nor YFP fluorophore was getting bleached by their respective lasers during standard imaging. The basic purpose of these series of "experiments" was to optimize the percentage transmission for each laser so that when performing FRET experiments in the future, I am not presented with false positive and/or false negative results.

In order to determine this setting, cells expressing hERG-mCFP or KvLQT1-mYFP were subjected to 100 scans at varying percent transmissions to the CFP and YFP lasers, respectively. The argon laser was set at 20% power. Five ROI points were placed on various cells: 4 were placed in cells that are expressing CFP or YFP and 1 in the background. The average intensities of the first 10 frames and last 10 frames were compared, and the percent change between these values was determined. The percentage transmission for the 458-nm laser was changed in 5% increments starting from 10% up to 40% to determine which percent transmission results in the most consistent levels of CFP intensities. The percentage transmission for the 514-nm laser was changed in 5% increments starting from 5% up to 40%, as well. Note that the YFP fluorophore is

considerably brighter in intensity compared to CFP to begin with. These optimization experiments were performed on Chinese Hamster Ovary (CHO) cells expressing the protein of interest.

At 40% transmission of the 458-nm laser, CFP expressing cells were over-exposed and there was extensive background noise in the images (Figure 6A). At 40% transmission of the 458-nm laser, CFP intensities steadily decreased after cells were exposed to 100 consecutive scans, suggesting that this percent transmission was photobleaching the CFP fluorophore (Figure 6B).

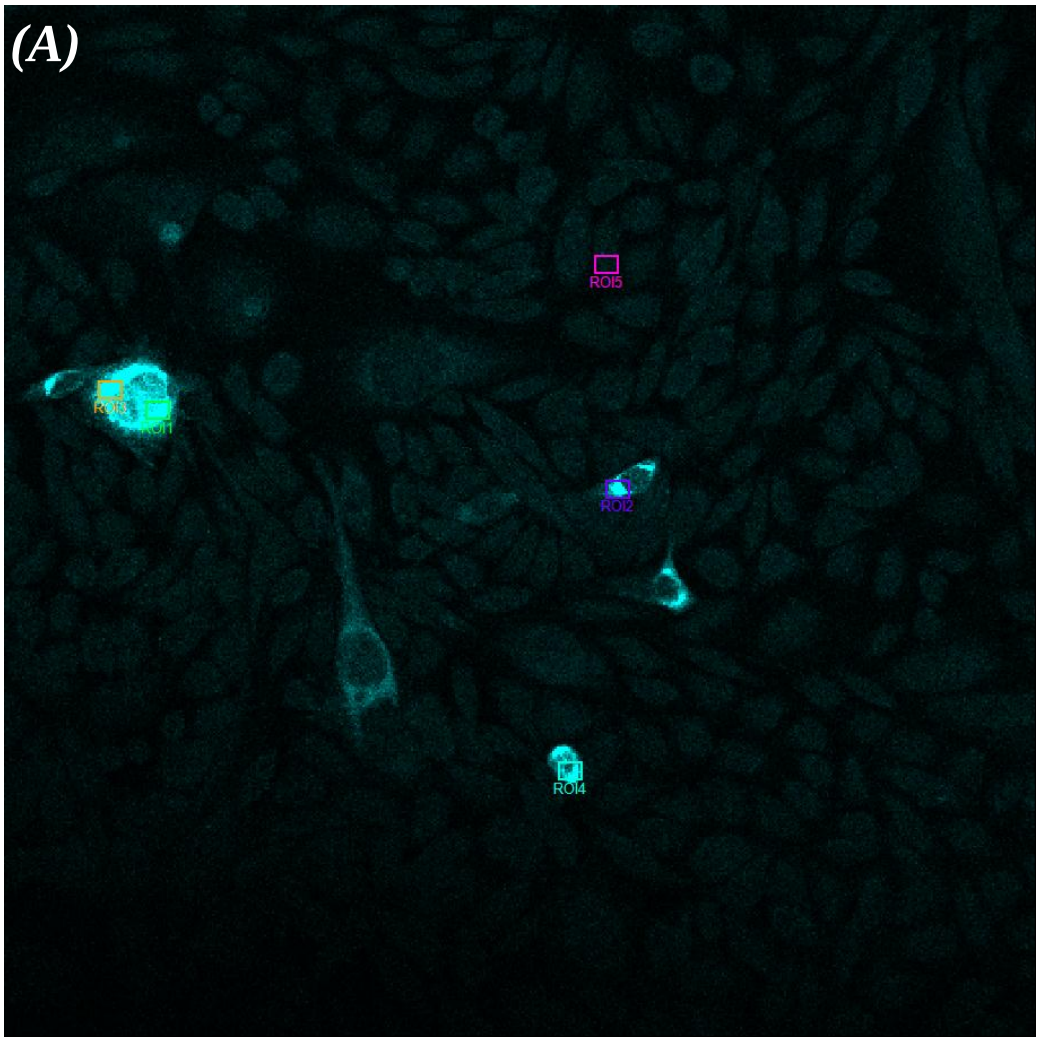

(B)

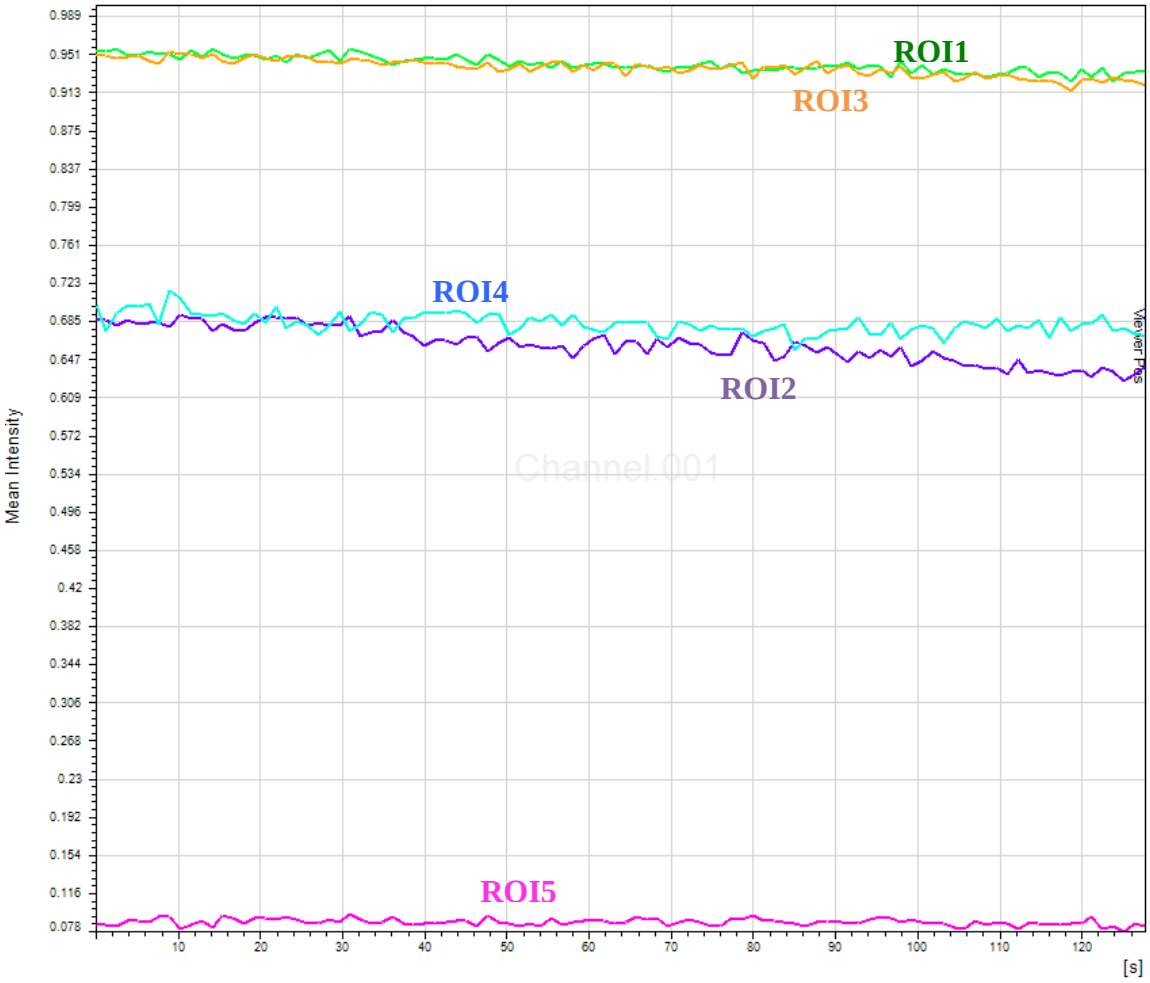

Average Intensities			
	First 10 frames	**Last 10 frames**	**Percent Difference**
ROI1	250.86	245.48	2.14
ROI2	180.55	167.04	7.48
ROI3	249.99	243.24	2.70
ROI4	183.77	178.87	2.66
ROI5	22.89	22.25	2.80

Figure 6. ***40% transmission of the 458 nm laser results in a noisy background for imaging and a relatively large percent change in CFP intensities over the course of 100 consecutive scans (129 s duration).*** (A) A representative image of CHO cells expressing hERG-mCFP. Five ROIs of the same size were placed throughout cells expressing CFP. One ROI (ROI5 in pink) was placed in the background with no CFP fluorescence as a control. (B) A normalized graph measuring mean intensities within the ROIs over the course of scans. The table below includes the average intensity within each ROI for the first and last 10 frames. The percent change was calculated. Images were taken on the 63X objective at 1X zoom and 1 Airy Unit on the confocal microscope. *Note:* Images shown here have been contrast enhanced for better qualitative visualization in this thesis.

The least amount of fluctuations in CFP intensities resulted at a percentage transmission of 20% of the 458-nm laser line (Figure 7).

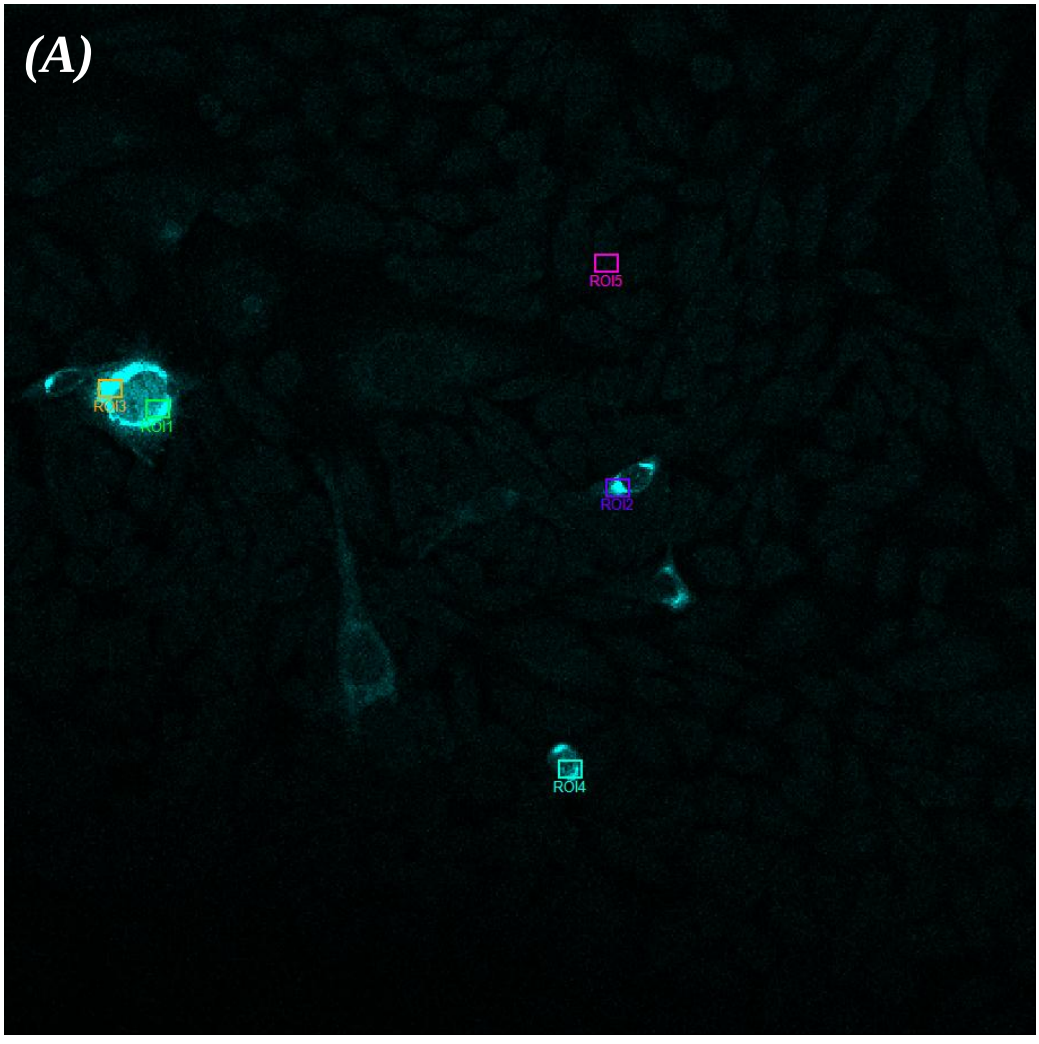

(B)

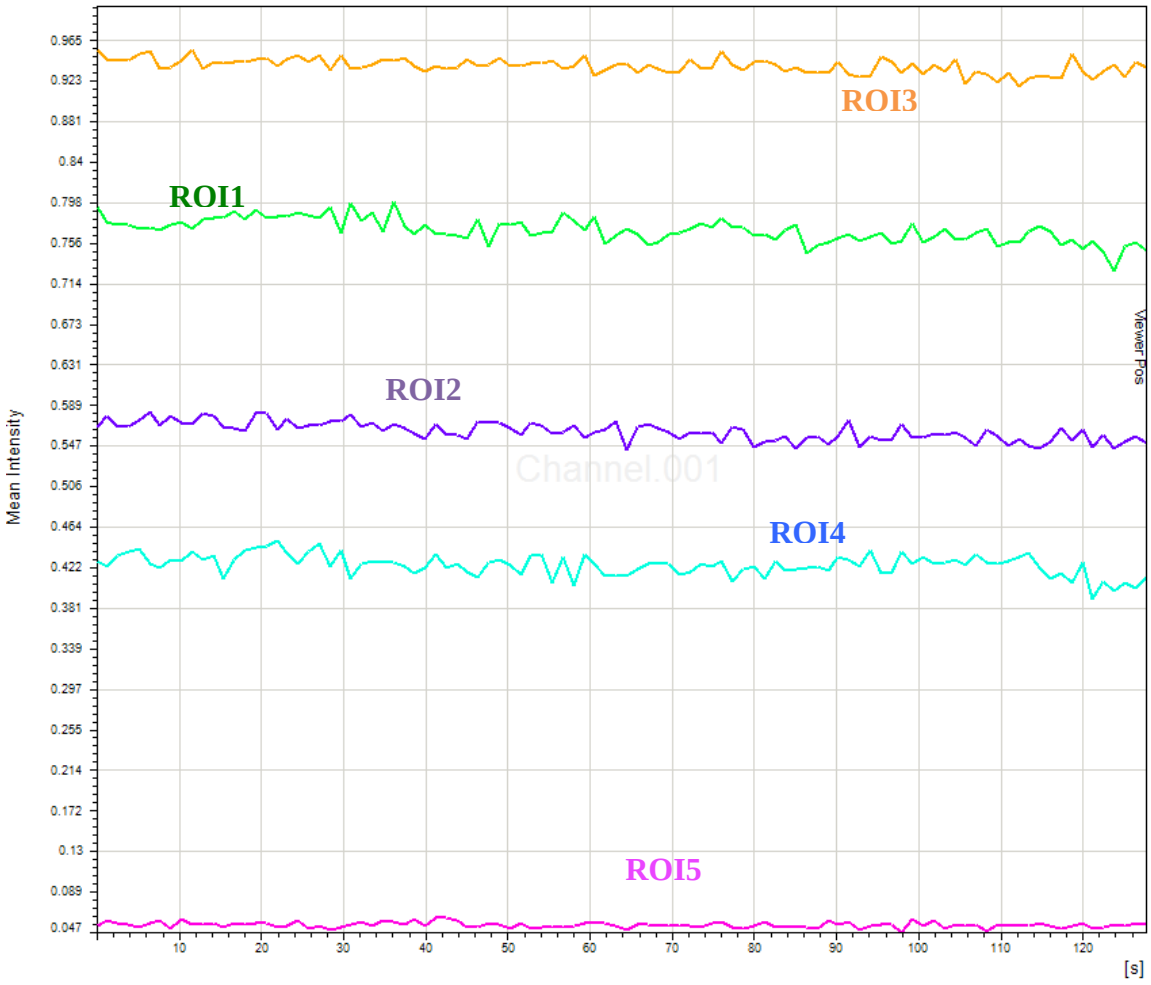

Average Intensities			
	First 10 frames	**Last 10 frames**	**Percent Difference**
ROI1	142.49	140.20	1.61
ROI2	105.40	104.35	1.01
ROI3	201.80	198.21	1.78
ROI4	61.81	60.70	1.80
ROI5	10.04	9.94	1.00

Figure 7. There is the least amount of fluctuation in CFP intensity when CFP is exposed to 458 nm laser line at 20% transmission for 100 consecutive scans (129 s duration). (A) A representative image of CHO cells expressing hERG-mCFP. Five ROIs of the same size were placed throughout cells expressing CFP. One ROI (ROI5 in pink) was placed in the background with no fluorescence as a control. (B) A graph measuring mean intensities within the ROIs over the course of scans. The table below includes the average intensity within each ROI for the first and last 10 frames. The percent change was calculated. Images were taken on the 63X objective at a zoom of 1X and 1 Airy Unit on the confocal microscope. *Note:* images were contrast enhanced for better visualization.

A similar series of experiments were performed on CHOs expressing KvLQT1-mYFP. The least amount of fluctuations in YFP intensities resulted at a percentage transmission of 10% of the 514-nm laser line (Figure 8). Note that while YFP intensity values themselves are quite low relative to the CFP intensity values, qualitatively YFP excited by the 514-nm laser at 10% transmission is brighter than CFP excited by the 458-nm laser at 20% transmission (Figures 7 and 8).

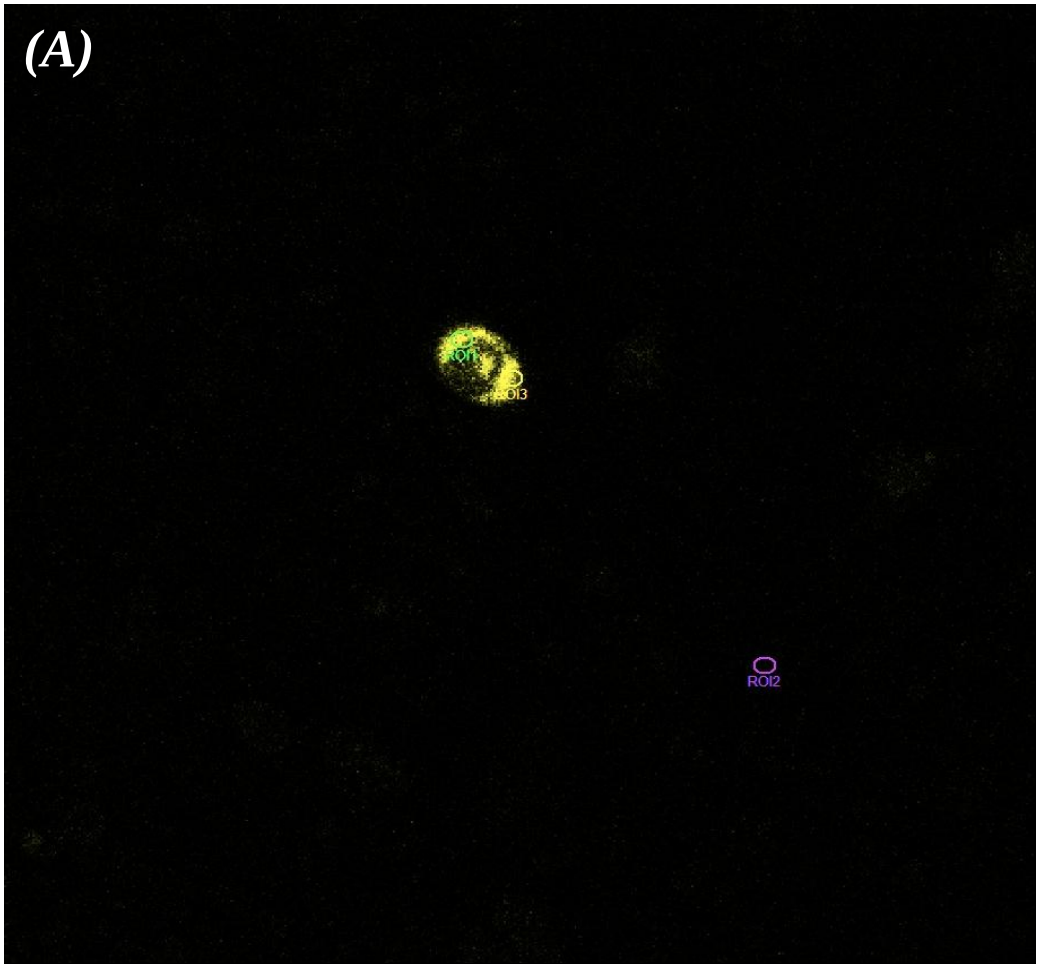
(A)
ROI1
ROI3
ROI2

(B)

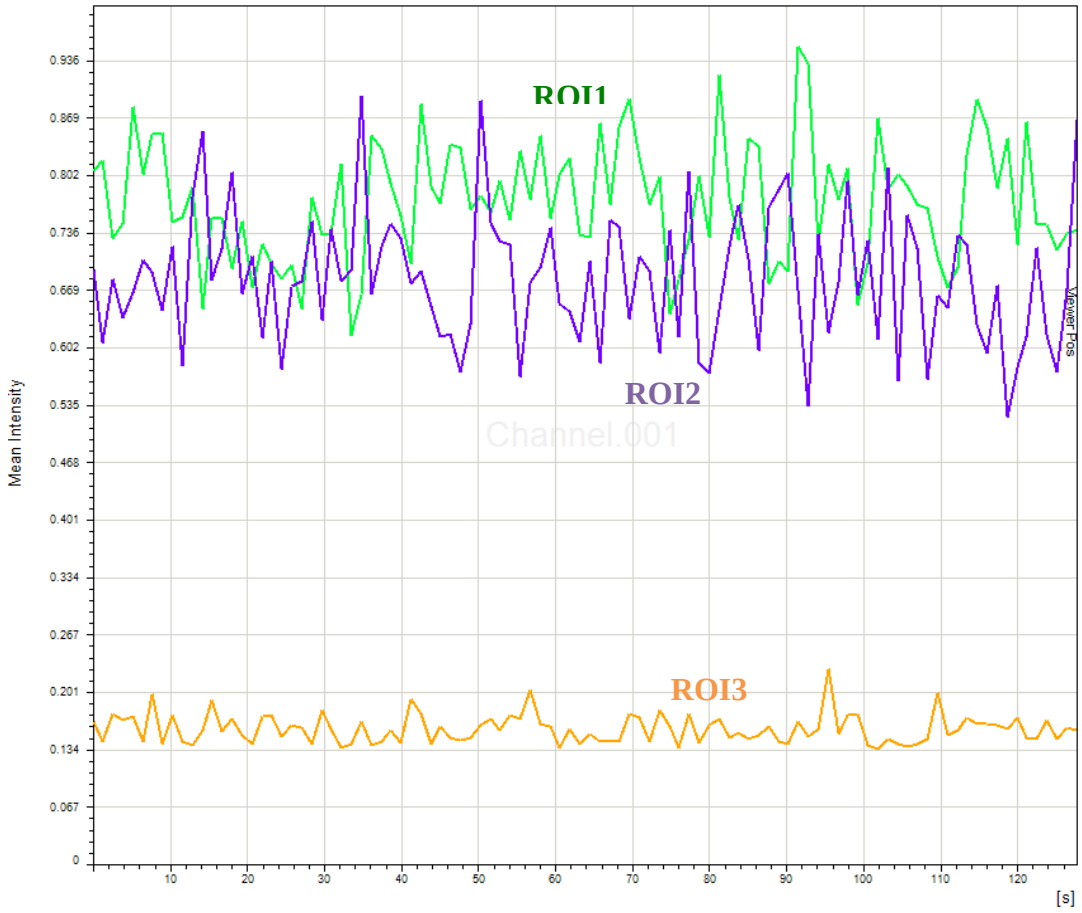

Average Intensities			
	First 10 frames	**Last 10 frames**	**Percent Difference**
ROI1	5.97	5.80	2.93
ROI2	4.95	4.81	2.88
ROI3	1.21	1.18	2.91

Figure 8. ***There is the least amount of fluctuation in YFP intensity when YFP fluorophore is exposed to 514 nm laser line at 10% transmission for 100 consecutive scans (129 s duration).*** (A) A representative image of CHO cells expressing KCNQ1-mYFP. Three ROIs of the same size were placed throughout cells expressing CFP. One ROI (ROI3 in purple) was placed in the background with no fluorescence as a control. (B) A graph measuring mean intensities within the ROIs over the course of scans. The table below includes the average intensity within each ROI for the first and last 10 frames. The percent change was calculated. Images were taken on the 63X objective at 1X zoom and 1 Airy Unit on the confocal microscope. *Note:* Images shown here have been contrast enhanced for better qualitative visualization in this thesis.

It was also necessary to address the issues of cross-excitation and emission bleedthrough between the CFP and YFP fluorophores. Upon excitation by the 458-nm laser, the CFP emission spectrum ranges from 460 to 535 nm. Upon excitation by the 514-nm laser, the YFP emission spectrum is measured from 580 to 650 nm. Their spectral overlap makes CFP and YFP a suitable FRET pair for apFRET experiments. Cross-excitation occurs when the donor (CFP) is excited by the acceptor (YFP) laser or when the acceptor molecule (YFP) is excited by the donor (CFP) laser. Emission bleedthrough occurs for similar reasons as crosstalk. The phenomenon generally occurs when the emission of one fluorophore is detected by the channel of the second fluorophore, for example if the donor (CFP) emission were detected by the acceptor (YFP) channel, and vice versa. The following questions were directly addressed: (1) Does the CFP laser excite YFP (cross-excitation), and vice versa? (2) Is CFP emission detected by the YFP channel (emission bleedthrough), and vice versa? Therefore, it was necessary to determine the boundaries of the emission spectrum for separate detection of CFP and YFP.

Initially, in order to address question (1) qualitatively, samples of CHOs expressing YFP (acceptor) only (KCNQ1-mYFP construct) were exposed to the 458-nm laser (CFP laser) at a 20% transmission. The YFP emission channel was turned on to see if the CFP laser was exciting YFP in the samples. The CFP emission detection range was arbitrarily set to 460–500 nm, and the YFP emission detection range was arbitrarily set to 580–650 nm. As shown in Figure 9, the CFP laser did not excite YFP within this YFP emission range.

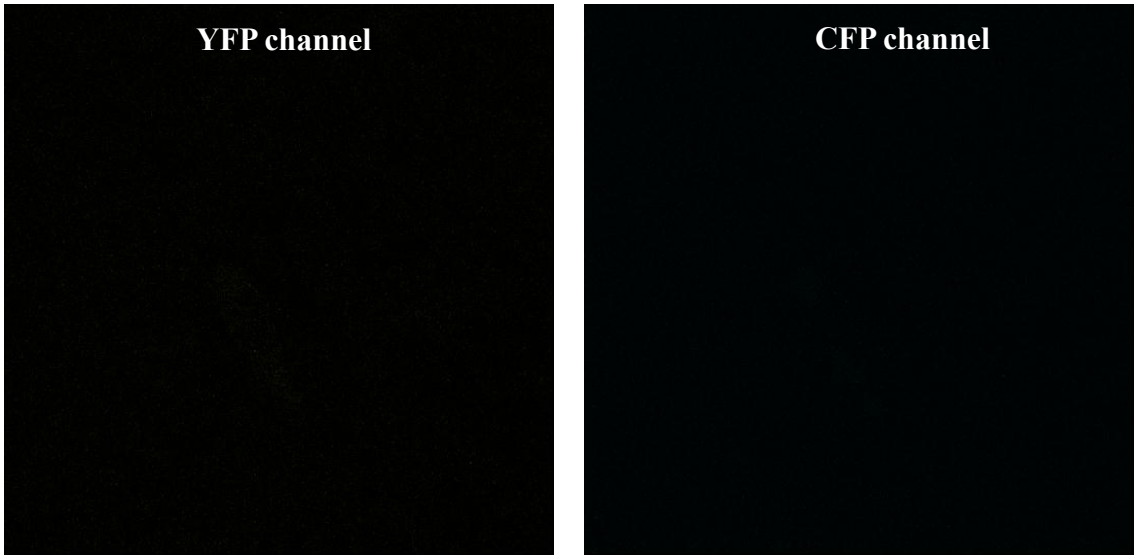

Figure 9. ***Cross-excitation of YFP by the CPF laser does not occur.*** CHO cell is expressing KvLQT1-mYFP. YFP and CFP emission channels are on. 458-nm laser was turned on and set at 20% transmission. CFP emission detection range: 460 nm–500 nm; YFP emission detection range: 580 nm–650 nm. Images were taken on the 63X objective at a zoom of 1X and 1 Airy Unit on the confocal microscope. *Note:* Images shown here have been contrast enhanced for better qualitative visualization in this thesis.

The corollary to question (1), specifically if the YFP laser excites CFP, was also addressed similarly. In this case, cells expressing CFP only (hERG-mCFP) were exposed to the 514-nm laser at 10% transmission. The CFP emission channel was turned on to see if the YFP laser was exciting CFP in these samples. The CFP and YFP emission detection ranges were set to 460–500 nm and 580–650 nm, respectively, as in the first experiment. The YFP laser also did not excite CFP, as CFP emission was not strongly detectable within this CFP emission range (data not shown).

In order to address question (2), samples of cells expressing CFP only (hERG-mCFP) were excited by the CFP laser at 20% transmission. Both the CFP and YFP channels were turned on to determine if CFP emission was detected by the set YFP

emission spectral range. The CFP and YFP emission detection ranges were set to 460–500 nm and 580–650 nm, respectively, as in the first experiment. CFP emission was detected by the CFP channel, as expected, but was not strongly detected by the YFP channel (Figure 10).

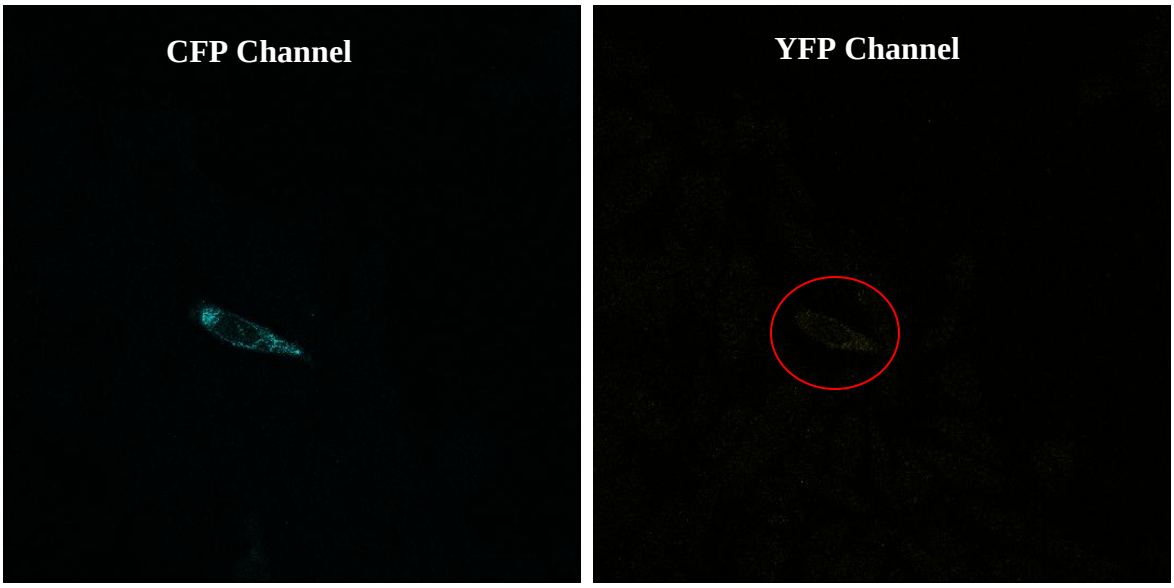

Figure 10. ***Emission bleedthrough of CFP as a result of CFP excitation into the YFP channel does not occur to a significant extent.*** CHO cell is expressing hERG-mCFP. YFP and CFP channels are on. 458-nm laser was turned on and set at 20% transmission. CFP emission detection range: 460 nm–500 nm; YFP emission range: 580 nm–650 nm. Images were taken on the 63X objective at a zoom of 1X and 1 Airy Unit on the confocal microscope. The red oval encompasses the minimal CFP emission bleedthrough detected in the YFP channel. *Note:* Images shown here have been contrast enhanced for better qualitative visualization in this thesis.

The same experiment was performed to test if YFP emission was detected by the CFP channel. In this case, cells expressing YFP only (KCNQ1-mYFP) were excited by the YFP laser at 10% transmission. Both the CFP and YFP emission channels were turned on to determine if YFP emission was detected by the set CFP emission spectral range. The CFP and YFP emission detection ranges were set to 460–500 nm and 580–650

nm, respectively, as in the first experiment. As shown in Figure 11, YFP emission from 514-nm laser excitement was not detected by the CFP channel.

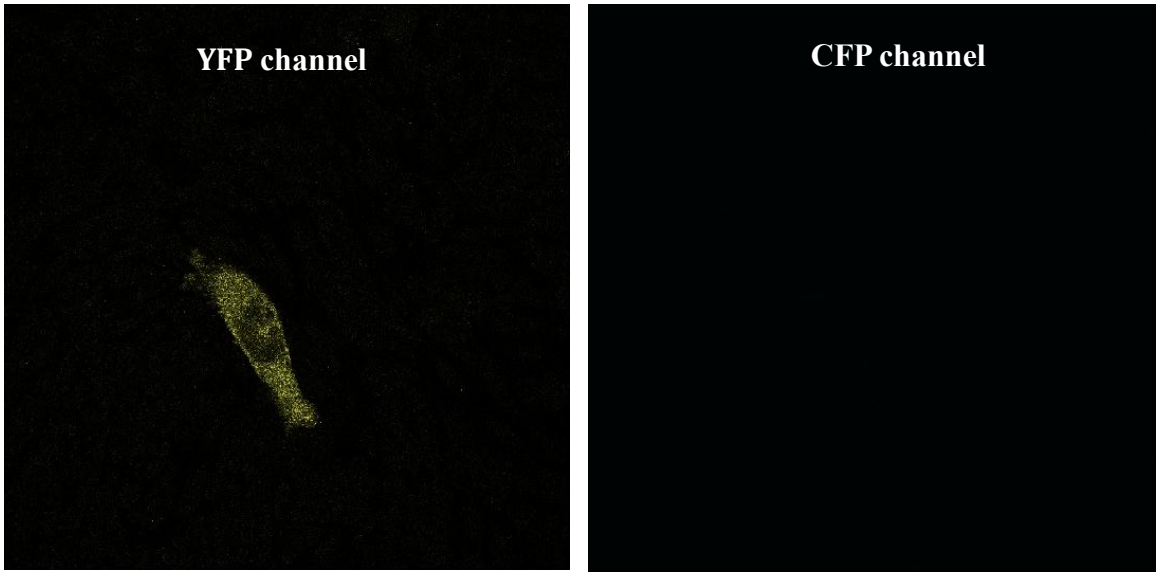

Figure 11. ***Emission bleedthrough of YFP as a result of YFP excitation into the CFP channel does not occur.*** CHO cell is expressing KvLQT1-mYFP. YFP and CFP channels are on. 514-nm laser was turned on and set at 10% transmission. CFP emission detection range: 460 nm–500 nm; YFP emission range: 580 nm–650 nm. Images were taken on the 63X objective at a zoom of 1X and 1 Airy Unit on the confocal microscope. *Note:* Images shown here have been contrast enhanced for better qualitative visualization in this thesis.

Furthermore, in order to determine the emission detection ranges for CFP and YFP that optimally minimize cross-excitation and emission bleedthrough, similar experiments were carried out as described above. In this case, the CFP-YFP linker soluble protein was expressed in CHOs, and each laser line was turned on individually with both the CFP and YFP channels on to determine the extent of detectable emission from each fluorophore by each laser. A total of 10 ROIs of the same dimensions were placed throughout the image field. Five ROIs were placed on cells that were fluorescing, while the other 5 were placed in the background (refer to Figure 12 for visualization of

the experimental setup). The average intensity values of the ROIs were compared between each channel. For example, the average CFP intensity values of the ROIs within cells and in the background were compared to the average YFP intensity values of these same ROIs when only the CFP laser was on. In this case with the CFP laser on, the CFP intensity values were expected to be significantly greater than the YFP intensity values, thus addressing the concept of cross-excitation and emission bleedthrough. CFP and YFP intensity values were also collected with the YFP laser on. In this case, the YFP intensity values were expected to be significantly greater than the CFP intensity values. Ultimately, CFP and YFP emission detection ranges of 470-510 nm and 580-650 nm, respectively, were determined to most effectively minimize cross-excitation and emission bleedthrough between the two fluorophores, as assessed by student's t-tests (Figure 12 and Table 1).

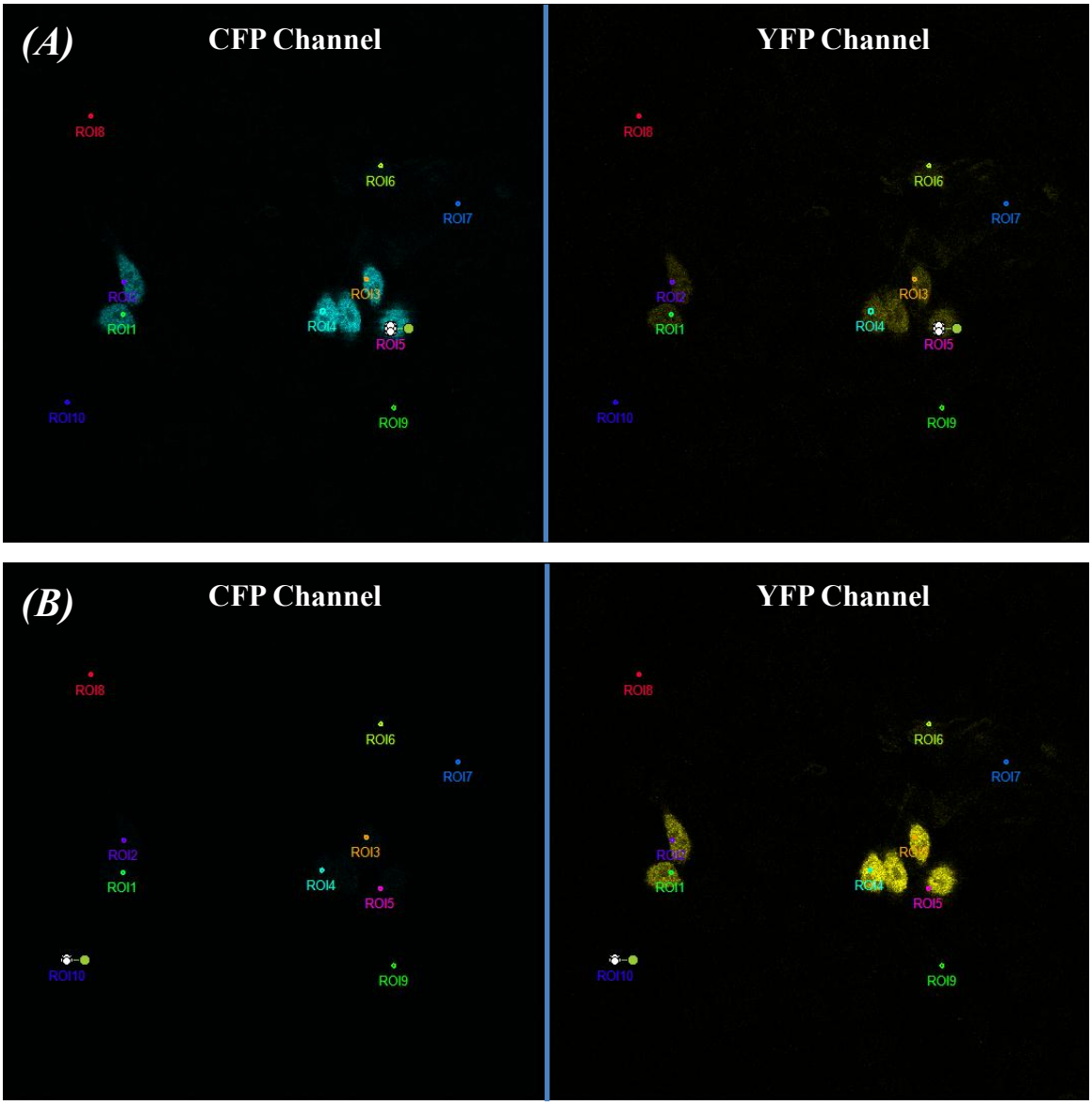

Figure 12. ***470-510 nm and 580-650 nm are the optimal ranges for CFP and YFP emission detection.*** CHO cells are expressing soluble CFP-YFP. The same field of view is presented in (A) and (B). (A) CPF laser on at 20% transmission. CFP and YFP emission channels on. The low-level signaling in the YFP channel is likely due to emission bleedthrough of CFP into the YFP channel, rather than cross-excitation of YFP by the CFP laser. (B) YFP laser on at 10% transmission. CFP and YFP emission channels on. ROIs 1-5 are placed on cells, ROIs 6-10 are placed throughout the background. Images were taken on the 63X objective at a zoom of 1 and 1 Airy Unit on confocal microscope. *Note:* Images shown here have been contrast enhanced for better qualitative visualization in this thesis.

Table 1 includes CFP and YFP intensity values corresponding to figures 11A and 11B. Average CFP intensity was significantly greater than YFP intensity within cells (student's t-test, $p < 0.001$). Average YFP intensity was significantly greater than CFP intensity within cells ($p < 0.001$)

CFP Laser On	*CFP Intensity*	*YFP Intensity*
ROI1	35.55	17.25
ROI2	34.7	10.7
ROI3	50.35	20.05
ROI4	51.6	16.95
ROI5	60.05	17.6
ROI6	5.45	4.95
ROI7	2.9	1.25
ROI8	3.2	3.9
ROI9	3.2	2.15
ROI10	4	5.9
YFP Laser on		
ROI1	4.1	27.8
ROI2	4.7	23.15
ROI3	5.15	38.7
ROI4	5.2	37.55
ROI5	3.45	37.75
ROI6	2	3.3
ROI7	2	1.05
ROI8	2.1	1.65
ROI9	2	1.1
ROI10	2	6.3

Optimization of Remaining FRET AB Parameters

Images for FRET experiments on the FRET AB Wizard were taken with the pinhole set at 1 Airy Unit, ensuring that true confocal images were taken, using a 63X 1.40 oil UV objective. The 514-nm laser line for the bleach step of the experiment was optimally set to 30% transmission. The average bleach depth observed at this transmission percentage in the experiments with the positive controls and experimental

FRET pairs was 87% ± 3.4% (mean ± SD). The number of frames of the bleach step was 5, which is equivalent to 5 seconds of exposure to the 514-nm laser. It is important to minimize the time it takes for bleaching because fluorophores are light sensitive molecules and thus will experience photobleaching when exposed to light for prolonged periods of time. Again, this is similar to why it was important to optimize the percent transmission to be utilized for each laser line (458-nm and 514-nm), so as to ensure that the corresponding fluorophore (CFP and YFP) experiences minimal photobleaching. The parameters utilized in the apFRET experiments in this study are presented in Table 2.

Table 2. *Leica FRET AB Wizard parameters utilized for apFRET experiments.*

Argon Laser Power: 20%		
63X objective/1.40 oil UV lens		
Speed: 400 Hz		
Pinhole: 95.51 µM (1 Airy unit)		
Zoom factor: 2		
CFP transmission: 20%	CFP emission range: 470-510 nm	CFP excitation: 458 nm laser
YFP transmission: 10%	YFP emission range: 580-650 nm	YFP excitation: 514 nm laser
Laser line for acceptor bleaching: 514 nm @ 30% transmission		
No. of frames: 5 (~5 s bleach time)		

apFRET Successfully Measures Interactions Between Wild-type hERG and KvLQT1

Cells from three different transfections were pooled into one sample group and imaged on 18 individual days to account for variability in transfection efficiency, cell passage number, and normal fluctuations in the imaging hardware. Ideally, 10 HEK cells expressing the protein(s) of interest were identified per slide, and no more than 1 slide per sample was examined in a sitting. Therefore, a maximum of 30 cells, with 10 cells from each sample group (i.e. positive control, negative control, and FRET pair), were pooled for each sample group from apFRET experiments.

HEKs were transfected with constructs for the wt condition: KCNQ1-CFP-YFP, hERG-mCFP, and hERG-mCFP + KCNQ1-mYFP, each in triplicate, which comprised a "single" transfection. A second and third round of transfections was also performed with these same constructs to allow for the variations discussed above and in case that not enough cells (at least 30) were present for apFRET experiments from the first round of transfection. The same procedures were followed for HEKs transfected with constructs for the mutant condition: KCNQ1-CFP-YFP, hERG-V822M-mCFP, and hERG-V822M-mCFP + KCNQ1-mYFP.

Average FRET efficiencies for experiments from all untreated and treated negative and treated positive controls for the wt and mutant conditions are presented in Table 3.

Table 3. *FRET efficiencies for all samples evaluated by apFRET.*

Donor	Acceptor	Treatment	E_f (%)	C_f (%)	*n*
Positive controls					
KCNQ1-CFP-YFP			25.8 ± 7.67	0.65 ± 1.15	30
KCNQ1-CFP-YFP		5 min; pCPT-cAMP + IBMX	26.7 ± 6.74	0.29 ± 0.65	30
KCNQ1-CFP-YFP			27.1 ± 6.26	2.74 ± 3.23	30
KCNQ1-CFP-YFP		5 min; pCPT-cAMP + IBMX	25.7 ± 6.70	1.39 ± 1.75	30
Negative controls					
hERG-mCFP			2.50 ± 3.72	0.60 ± 1.53	30
hERG-mCFP		5 min; pCPT-cAMP + IBMX	2.43 ± 2.46	0.18 ± 0.32	30
hERG-V822M-mCFP			3.52 ± 3.33	0.96 ± 1.38	30
hERG-V822M-mCFP		5 min; pCPT-cAMP + IBMX	2.04 ± 2.42	0.49 ± 0.89	30
Experimental FRET pairs					
hERG-mCFP	KCNQ1-mYFP		10.3 ± 3.44	0.49 ± 0.96	30
hERG-mCFP	KCNQ1-mYFP	5 min; pCPT-cAMP + IBMX	5.49 ± 3.19	0.06 ± 0.21	30
hERG-V822M-mCFP	KCNQ1-mYFP		5.93 ± 3.84	1.18 ± 1.40	30
hERG-V822M-mCFP	KCNQ1-mYFP	5 min; pCPT-cAMP + IBMX	5.57 ± 2.93	0.80 ± 1.10	30

Values are mean ± SD. E_f, FRET efficiency; C_f, control for false-positive FRET efficiency.

Firstly, we were interested in determining if apFRET was an effective method for measuring interactions between wt hERG and KvLQT1. We expected that the FRET efficiencies of experimental regions of the positive control, negative control, and wt FRET pair would be significantly different from one another. Histograms of the FRET efficiencies in the experimental and control regions of individual cells demonstrate distinct populations of FRET efficiencies in positive controls in both untreated and treated conditions, as expected because FRET should occur in the experimental regions but not in the control regions in both treatment conditions, for the donor and acceptor are directly linked in this case (Figure 13).

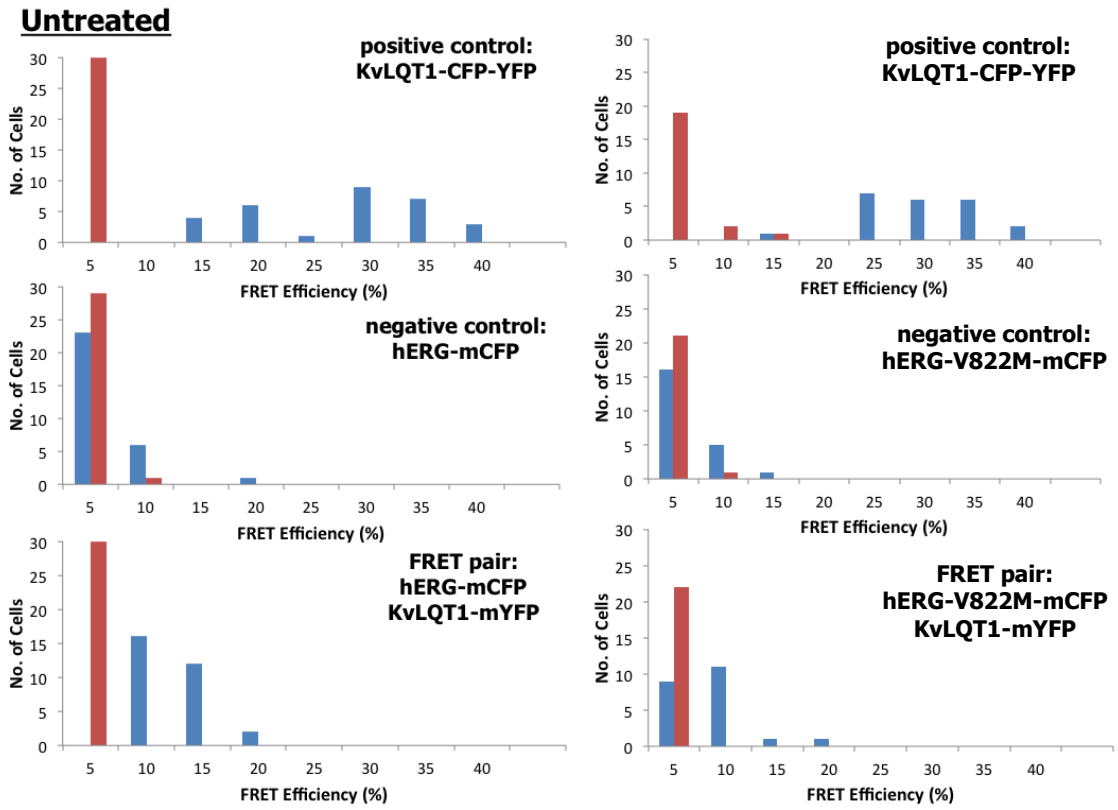
Untreated
positive control:
KvLQT1-CFP-YFP
negative control:
hERG-mCFP
FRET pair:
hERG-mCFP
KvLQT1-mYFP
positive control:
KvLQT1-CFP-YFP
negative control:
hERG-V822M-mCFP
FRET pair:
hERG-V822M-mCFP
KvLQT1-mYFP
No. of Cells
FRET Efficiency (%)

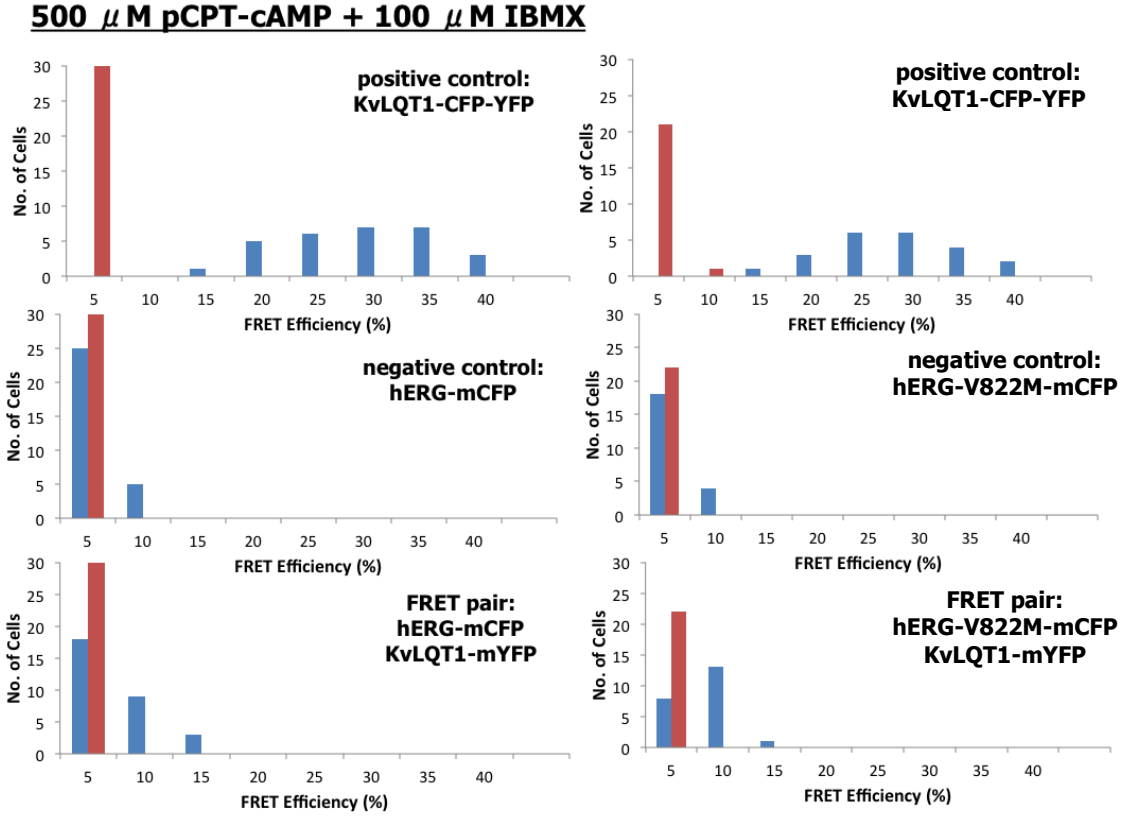
500 μM pCPT-cAMP + 100 μM IBMX
positive control:
KvLQT1-CFP-YFP
negative control:
hERG-mCFP
FRET pair:
hERG-mCFP
KvLQT1-mYFP
positive control:
KvLQT1-CFP-YFP
negative control:
hERG-V822M-mCFP
FRET pair:
hERG-V822M-mCFP
KvLQT1-mYFP
No. of Cells
FRET Efficiency (%)

Figure 13. ***Elevated cAMP levels abrogate wt hERG-KvLQT1 interactions, while mutant hERG-wt KvLQT1 interactions remain unchanged.*** Individual E_f and C_f values from each positive control, negative control, and FRET pair groups (wt and V822M hERG mutant) were plotted onto histograms. Top half represents data from all untreated samples, bottom half represents data from all samples treated with 500 μM pCPT-cAMP and 100 μM IBMX. Cells were treated for 5 minutes. Left column represents data from positive control, negative control, and FRET pair of wt hERG and KvLQT1. Right column represents data from positive control, negative control, and FRET pair of V822M hERG and wt KvLQT1. **Blue** and **red** bars represent **bleached** and **control** (unbleached) ROIs, respectively, within the same cell (*n*=30 for each sample set). Data was collected from cells pooled together from multiple transfections and imaged over multiple sessions.

This distinction is not observed in the histograms for FRET efficiencies of the negative control samples, as expected (Figure 13). Positive controls demonstrated intramolecular FRET between the CFP and YFP fluorophores directly linked together via a short peptide sequence. Negative controls demonstrated no significant change in CFP emission in the absence of YFP, leading to very low values for FRET efficiencies and providing a sensitivity threshold for establishing protein-protein interactions. Figure 14 demonstrates the same trends between the untreated and treated conditions of the positive and negative controls as observed in the histograms in Figure 13, but in box plots.

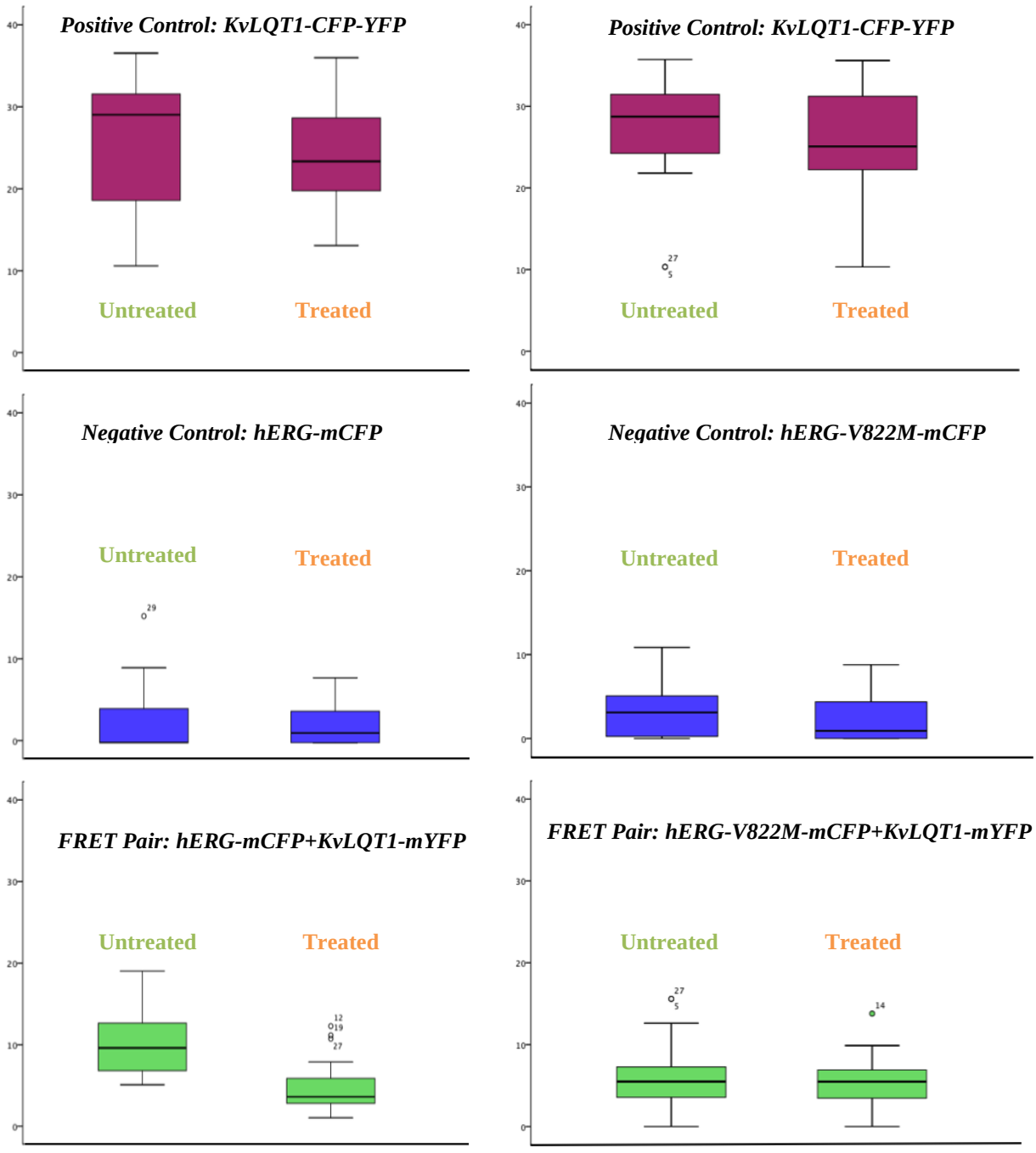

Figure 14. ***Data set from Figure 12 presented in box plots.*** Pink, blue, and green bars represent the positive control, negative control, and FRET pairs, respectively.

A 3-factor ANOVA with no interactions between the factors of treatment (untreated vs. treated), group (positive control, negative control, FRET pair), and mutant (wt hERG or V822M hERG) was performed in order to determine the effect of these 3 conditions on FRET efficiency across all samples. The ANOVA was performed on FRET efficiency values from experimental regions only. A significant effect due to group type was observed ($p < 0.001$). Thus, we proceeded to make comparisons between mean E_f values of the positive control, negative control, and wt FRET pair using individual student's t-tests.

The mean E_f of the positive control was significantly greater than the mean E_f of both the negative control and the wt FRET pair ($p < 0.05$), as determined by student's t-tests. The mean E_f of the negative control was significantly less than the mean E_f of the wt FRET pair ($p < 0.05$), as determined by student's t-tests. The mean E_f of the positive control was significantly greater than the mean E_f of the wt FRET pair ($p < 0.05$), as determined by student's t-tests. This makes sense because in the positive control, the CFP and YFP fluorophores were directly fused together. Therefore, the E_f values of the wt positive control represent the maximum FRET efficiency that can be measured in this experimental and hardware design. Additionally, E_f cannot be 100% because the fluorophores physically take up space due to their size, and as a result, there will always be some distance between them. In the case of the wt FRET pair, the two proteins are co-expressed, and therefore the CFP and YFP fluorophores would be localized even further away from each other than if the two were fused together.

Elevated cAMP Levels Modulate FRET Efficiencies Between Wild-type hERG and KvLQT1

Average FRET efficiencies in untreated and pCPT-cAMP + IBMX treated HEKs expressing KvLQT1-CFP-YFP (positive control) were 25.8 ± 7.67% and 26.7 ± 6.74%, respectively. Average FRET efficiencies in the control regions in untreated and treated HEKs expressing KvLQT1-CFP-YFP were 0.65 ± 1.15% and 0.29 ± 0.65%, respectively.

Average FRET efficiencies in untreated and treated HEKs expressing hERG-mCFP (negative control) were 2.50 ± 3.72% and 2.43 ± 2.46%, respectively. Average FRET efficiencies in the control regions of untreated and treated HEKs expressing hERG-mCFP were 0.60 ± 1.53% and 0.18 ± 0.32%, respectively. pCPT-cAMP + IBMX treatment did not significantly affect FRET efficiencies in the positive and negative controls, as expected (Figure 14).

Mediation of hERG-KvLQT1 interactions by cAMP may demonstrate the physiological regulation of these protein interactions. Because we hypothesized that cAMP directly binds to the CNBhD on the COOH-terminus of hERG, we wanted to first assess the overall effects elevated cAMP on hERG-KvLQT1 interactions to confirm whether cAMP plays a role at all. In order to address the role of intracellular cAMP on the interactions between hERG and KvLQT1, HEKs co-expressing wt hERG and KvLQT1 were exposed to pCPT-cAMP and IBMX treatment for 5 minutes in order to elevate intracellular cAMP levels as would physiologically occur in response to sympathetic stimulation.

Because a significant effect due to pCPT-cAMP and IBMX treatment ($p < 0.01$) was observed in the ANOVA, we were able to make within-group comparisons between

the FRET efficiencies of the untreated and treated wt FRET pair using a student's t-test. Average FRET efficiencies in untreated and treated HEKs co-expressing wt hERG-mCFP and KvLQT1-mYFP were 10.3 ± 3.44 and 5.49 ± 3.19, respectively. Average FRET efficiencies in the control regions of untreated and treated HEKs expressing hERG-mCFP were 0.49 ± 0.96 and 0.06 ± 0.21, respectively. Thus, pCPT-cAMP + IBMX treatment resulted in a significant, 48% reduction in FRET efficiency in the wt FRET pair ($p < 0.05$). These results support the hypothesis that cAMP levels modulate the direct interactions between wt hERG and KvLQT1.

Elevated cAMP Levels Do Not Affect FRET Efficiencies Between V822M hERG Mutant and Wild-type KvLQT1

Average FRET efficiencies in untreated and pCPT-cAMP treated HEKs expressing KvLQT1-CFP-YFP (positive control for the V822M hERG mutant) were 27.1 ± 6.26% and 25.7 ± 6.70%, respectively. Average FRET efficiencies in the control regions in the same untreated and treated HEKs expressing KvLQT1-CFP-YFP were 2.74 ± 3.23% and 1.39 ± 1.75%, respectively. Note that these average C_f values are significantly greater ($p < 0.05$) than the C_f values collected from the positive controls for the wt FRET pair, based on student's t-tests. This may be due to issues with the machinery (microscope or laser) because the same construct was used as the positive control for both the wt and mutant FRET pairs. It would be worthwhile to create a new set of untreated and treated samples of all the constructs and perform another run of the experiments detailed in this thesis to determine if these variations in C_f values are normal before proceeding with future apFRET experiments. These differences could also be due to an experimenter bias introduced inherently when picking cells to perform the apFRET

experiments. It may be that the cells with the greater C_f values represent a sample of brighter-intensity cells at baseline compared to the cells with the lower C_f values. This potential issue of experimenter bias should also be addressed in future apFRET studies to determine if there is an effect of fluorescence intensity on FRET efficiency and to ensure that cells with high-intensity of fluorescence are not overly selected.

Average FRET efficiencies in untreated and treated HEKs expressing hERG-V822M-mCFP (negative control) were 3.52 ± 3.33% and 2.04 ± 2.42%, respectively. Average FRET efficiencies in the control regions of untreated and treated HEKs expressing hERG-V822M-mCFP were 0.96 ± 1.38 and 0.49 ± 0.89, respectively. pCPT-cAMP and IBMX treatment did not significantly affect FRET efficiencies in the positive and negative controls, as expected (Figure 14).

We hypothesized that cAMP plays a direct role in modulating the interactions between hERG and KvLQT1 through direct binding at the conserved CNBhD on the COOH-terminus of hERG versus an indirect role through the activation of PKA. In order to address the molecular mechanism through which cAMP induces its effects on the mediation of hERG-KvLQT1 interactions, the same series of apFRET experiments were performed on HEKs expressing the V822M mutant hERG and wt KvLQT1. The V822M mutation located in the CNBhD of hERG renders the domain functionless, thereby preventing cAMP from binding (Satler et al., 1996; Cui et al., 2001). HEKs co-expressing hERG-V822M-mCFP and KvLQT1-mYFP were treated with pCPT-cAMP and IBMX for 5 minutes to acutely elevate intracellular cAMP levels, as was done in cells co-expressing wt hERG and KvLQT1. We wanted to compare the mean E_f values of the

untreated and treated mutant FRET pair (hERG-V822M-mCFP + KvLQT1-mYFP), and we expected that there would be no significant difference between these values.

Average FRET efficiencies in untreated and treated HEKs co-expressing hERG-V822M-mCFP and wt KvLQT1-mYFP were 5.93 ± 3.84% and 5.57 ± 2.93%, respectively. Average FRET efficiencies in the control regions of untreated and treated HEKs expressing hERG-V822M-mCFP and wt KvLQT1-mYFP were 1.18 ± 1.40% and 0.80 ± 1.10%, respectively. Based on the significant effect of group type and treatment type observed in the 3-factor ANOVA, we made within-group comparisons between untreated and treated mutant FRET pairs using student's t-tests. pCPT-cAMP + IBMX treatment did not significantly change FRET efficiencies in the mutant FRET pair. These results tentatively demonstrate that elevated cAMP levels were unable to reduce the interactions between V822M hERG and KvLQT1.

The Overall Effect of Elevated cAMP Levels on FRET Efficiencies Between Wild-type and CNBhD Mutant FRET Pairs is Inconclusive

We were also interested in making a between-groups comparison between the mean E_f values of the treated wt FRET pair and the treated mutant FRET pair. We expected that the mean E_f value of the wt FRET pair for the treated condition would be significantly less than that of the mutant FRET pair for the same condition because the same interactions present in both of the untreated wt and mutant FRET pairs should not have been affected in the treated mutant FRET pair. No significant effect of mutant-type was initially observed in the 3-factor ANOVA. This result was not expected initially, but the lack of a significant effect makes sense because the 3-factor ANOVA included all of E_f values for the positive and negative controls, in addition to the E_f values for the wt

FRET pair. Therefore, in order to address the question above, a 2-factor ANOVA of the E_f values of the FRET pairs only was performed. The factors were treatment-type (untreated or pCPT-cAMP + IBMX treated) and mutant-type (wt or V822M hERG mutant). Narrowing down the data to include only the E_f values of the experimental FRET pairs, and thus taking out the group-type factor, helped to more precisely analyze the effects of treatment on hERG-KvLQT1 interactions. A significant effect of mutant-type was observed ($p < 0.001$). A significant effect of treatment-type was also observed ($p < 0.001$).

We went on to perform a student's t-test between the mean E_f values of the treated wt and mutant FRET pairs. Student's t-tests demonstrated that the average FRET efficiency of the wt FRET pair was significantly reduced with pCPT-cAMP and IBMX treatment ($p < 0.05$), while the average FRET efficiency of the FRET pair including the CNBhD mutant (hERG V822M) was unaffected by the same treatment ($p < 0.05$). However, the average FRET efficiency of the untreated CNBhD mutant FRET pair was significantly lower than the average FRET efficiency of the wt FRET pair ($p < 0.05$), suggesting that the CNBhD mutant (hERG V822M) may not associate with KvLQT1 to the same extent as wt hERG (Figure 15). Therefore, direct comparisons of treatment effect between the wt and CNBhD mutant FRET pairs are not valid based on this experimental design.

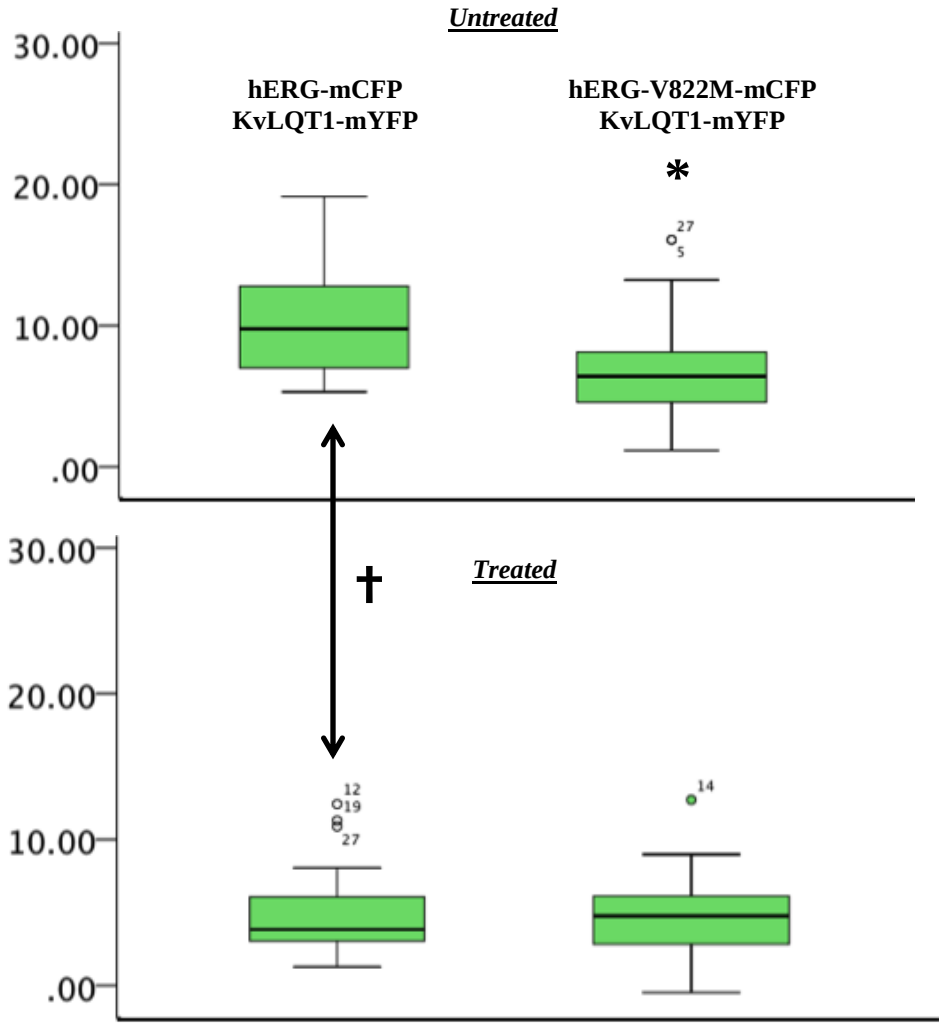

Figure 15. ***Overall effect of elevated cAMP levels on FRET efficiencies between wt and CNBhD mutant FRET pairs is inconclusive.*** Green bars represent the FRET pairs of the data set in figure 12. Left column represents wt FRET pairs, right column represents mutant FRET pairs. Untreated: no pCPT-cAMP+IBMX; treated: 500 µM pCPT-cAMP + 100 µM IBMX for 5 min. A 2-factor ANOVA was performed, followed by student's t-tests within and between groups. † indicates statistical significance ($p < 0.05$) between untreated and treated sample groups. ***** indicates statistical significance ($p < 0.05$) wt and mutant FRET pairs.

Discussion

The main goal of this study was to address the following hypothesis: Direct interactions between the α-subunit cardiac potassium channel proteins hERG and KvLQT1 are modulated by direct binding of cAMP to the CNBhD located on the COOH-terminus of hERG. My first aim was to affirm that increased intracellular cAMP levels diminished wt hERG and KvLQT1 interactions using the Leica SP5 II confocal system. My second aim was to address the effects of elevated intracellular cAMP levels on V822M hERG mutant and wt KvLQT1 interactions. These proteins were expressed in HEK cells, and their interactions were assessed via apFRET experiments. Troubleshooting and optimization of apFRET parameters on the FRET AB Wizard of the Leica TCS SP5 II was essential, as apFRET experiments had not previously been performed on the current Leica system (Organ-Darling et al., 2013). I was able to successfully establish FRET AB parameters that were utilized throughout the series of experiments in this study.

Wt FRET pairs with elevated cAMP levels were expected to have significantly decreased FRET efficiencies compared to "normal" cAMP levels, while the FRET efficiencies were not expected to be significantly different in the untreated and treated mutant FRET pairs. This is because it was originally hypothesized that cAMP directly binds to the CNBhD, thereby abrogating the direct interactions between hERG and KvLQT1, as assessed by a decrease in FRET efficiency. Therefore, in the wt FRET pair, it was expected that increasing intracellular cAMP levels with acute pCPT-cAMP + IBMX treatment would result in a significant decrease in FRET efficiency compared to the untreated condition. In the mutant FRET pair with the V822M hERG mutant that

possesses a non-functioning CNBhD, it was expected that increasing intracellular cAMP levels with the same treatment would not result in significant differences in FRET efficiencies from the untreated condition because cAMP would no longer bind to this domain to abrogate the interactions.

A 3-factor ANOVA without interactions was performed to determine the effects of group-type, treatment-type, and mutant-type on FRET efficiencies. Significant effects imply that the means within each type differ more than would be expected by chance alone. Overall, treatment-type and group-type demonstrated significant effects on FRET efficiency. No significant effect on FRET efficiency was present within the mutant-type condition. Therefore, we proceeded to perform individual t-tests to make within-group comparisons between the mean E_f value of the untreated and treated wt FRET pair, and between the E_f value of the untreated and treated mutant FRET pair.

Based on our current statistical analyses, FRET efficiency in pCPT-cAMP + IBMX treated HEKs expressing wt hERG and KvLQT1 was significantly lower than in untreated HEKs expressing the wt FRET pair. FRET efficiency in treated HEKs expressing the V822M hERG mutant and wt KvLQT1 was not significantly different from the FRET efficiency observed in untreated cells expressing the mutant FRET pair. These results were in accordance with the proposed expectations.

A 2-factor ANOVA without interactions was also performed to determine the effects of treatment-type and group-type on FRET efficiencies of the wt and mutant FRET pairs only. While the first 3-factor ANOVA did not produce any significant effect of mutant-type on FRET efficiency, this may have been due to the fact that the FRET efficiencies of the positive and negative controls were included in the analysis. These

values should generally not change between wt and mutant conditions, and therefore may have attributed to the lack of significance. Thus, we narrowed down our data pool to include only the FRET efficiencies of the experimental wt and mutant FRET pairs in the 2-factor ANOVA. Overall, treatment-type and mutant-type demonstrated significant effects on FRET efficiencies of the wt and mutant FRET pairs. Therefore, we proceeded to perform individual t-tests to make a between-group comparison between the FRET efficiency of the wt and mutant FRET pairs in the treated condition.

We expected the FRET efficiency of the treated wt FRET pairs to be significantly lower than that of the treated mutant FRET pairs, assuming that the untreated wt and mutant FRET pairs exhibit the same baseline FRET efficiencies. Based on a student's t-test, the mean E_f values of the treated wt and mutant FRET pairs were not significantly different. However, this is due to the fact that the mean E_f values of the untreated wt and mutant FRET pairs were significantly different from one another ($p < 0.05$), based on a student's t-test. Thus, we were unable to validly make this specific comparison. This difference was unexpected because we assumed, based on previous literature reports, that the V822M hERG mutant was essentially the same as wt hERG in all aspects except for the loss of function of the CNBhD (Cui et al., 2001). Therefore, we did not expect the V822M hERG mutant to bind cAMP, but we did expect it to traffic normally through the secretory pathway and localize normally to the cell membrane. However, we observed that there were some unexpected trafficking issues with the V822M mutant. Qualitatively, the mutant hERG did not appear to traffic successfully to the cell membrane and was not distributed evenly throughout the cell compared to wt hERG trafficking.

Because the FRET efficiencies for the wt and mutant FRET pairs in the untreated condition were significantly different from one another, comparisons between treated wt and treated mutant FRET pairs cannot be made with confidence and the biological significance of statistical tests is unclear. However, because the results appear skewed due to an intrinsic, unexpected problem with the V822M mutant, the ANOVA does not accurately account for the unexpected variance in the FRET efficiencies of the untreated mutant FRET pair. Because there is initially an unexpected significant difference between the FRET efficiencies of the untreated wt and mutant FRET pairs, further comparisons could not be made with confidence.

One important factor to consider when discussing the discrepancy in the expected and actual results is the trafficking of the V822M hERG mutant. Mutations in the CNBhD of hERG have been attributed to its inability to bind cyclic nucleotides and/or its improper trafficking (Cui et al., 2001). The reason we chose to work with the V822M mutant hERG was because we expected normal trafficking of the mutant to the membrane (Cui et al., 2001), and therefore we expected that FRET efficiencies would be similar between the wt and mutant FRET pairs. However, this was not the case. Additionally, when cells expressing the hERG mutant were visualized on the confocal microscope, hERG trafficking appeared to be disrupted based on the presence of punctate clusters and/or accumulations of CFP throughout the cell before reaching the membrane. These clusters are also usually "bright" spots on imaging, often reaching saturated values under our standard imaging protocols. Saturation poses an issue for quantification of images as you have effectively capped one end of the dynamic range of detection. The

expression of CFP in cells expressing the hERG mutant was not as homogenous as in cells expressing wt hERG-mCFP.

The results corresponding to the wt FRET pair are in accordance with expectations as well as with the results of previous studies. Organ-Darling et al. (2013) also found that elevated intracellular cAMP levels resulted in decreased FRET efficiency in cells expressing wt hERG and KvLQT1. Cui et al. (2000) saw that K^+ current amplitude decreased within 3 minutes of pCPT-cAMP application, and more specifically that I_{Kr} decreased by 40%, suggesting that cAMP plays a role in hERG function.

These data do not necessarily confirm my initial hypothesis, but it also does not refute the alternative hypothesis involving the role of PKA phosphorylation of either hERG or KvLQT1, or both. Even in the presence of a mutated, nonfunctional CNBhD, the effects of elevated cAMP could still have resulted in hERG-KvLQT1 interaction abrogation via PKA activation and phosphorylation of either or both of these channels.

In light of recent literature reports and growing consensus in the field, we adopt the alternative hypothesis that direct hERG-KvLQT1 interactions are modulated by cAMP-dependent PKA phosphorylation of either hERG or KvLQT1, or both. There is increasing evidence in favor of the PKA-mediated mechanism over the direct role of the CNBhD. Firstly, there is convincing structural, biophysical, and electrophysiological data supporting the view that the CNBhD of KCNH channels, including hERG, does not physically bind cyclic nucleotides. As introduced earlier, Brelidze et al., Marques-Carvalho et al., and Li et al. have demonstrated evidence that cyclic nucleotides do not directly bind to the CNBhD (Brelidze et al., 2009; Marques-Carvalho et al., 2012; Li et al., 2014). Other potential functions of the CNBhD are possible. Rather than binding

cyclic nucleotides, it has been shown that the CNBhDs in KCNH channels bind other ligands, particularly intrinsic ligands, which regulate channel activity (Haitin et al., 2013; Gustina and Trudeau, 2011). Interestingly, Haitin et al. (2013) showed that the CNBhD of KCNH channels instead interact directly with the eag domain of the amino terminus to regulate channel function and gating kinetics. There have also been reports that the Per-Arnt-Sim (PAS) domain in the cytoplasmic amino-terminal region of hERG directly interacts with the CNBhD in the COOH-terminus, thereby regulating slow deactivation of the channel (Gustina and Trudeau, 2011). These findings suggest that the CNBhD may have evolved other functions that are more directly involved in regulating KCNH channel activity.

Secondly, the mechanism of the cAMP-dependent PKA-mediated phosphorylation of KCNH2 channels has been relatively well delineated. There are 4 identified PKA phosphorylation sites located on hERG: aa 283, 890, 895, and 1137 (Thomas et al., 1999). Amino acids 890 and 895 are located within the CNBhD. This already indicates to us that PKA phosphorylation of hERG occurs. Thomas et al. (1999) mutated the PKA phosphorylation sites to alanines and showed that this inhibited hERG activation. Utilizing that same phosphonull mutants, PKA inhibitors, immunoprecipitation, and electrophysiology, Cui et al. (2000) also demonstrated that cAMP-dependent PKA phosphorylation of hERG occurs, resulting in accelerated deactivation and a rightward shift in voltage dependence of activation, making the channel less likely to open in response to an action potential. Chen et al. (2009) also demonstrated that PKA phosphorylation of hERG as a result of elevated intracellular cAMP levels augmented channel synthesis, illustrating that PKA phosphorylation of

hERG does likely occur and is involved in a variety of cellular functions (Chen et al., 2009).

However, the role of PKA phosphorylation of hERG on modulating hERG-KvLQT1 interactions is still unclear, and therefore a biological question to be addressed by the Darling lab. β-adrenergic stimulation via cAMP/PKA-dependent pathways attenuates I_{Kr}, while it enhances I_{Ks} (Cheng et al., 2014). This suggests that the phosphorylation of hERG may somehow disrupt interactions between hERG and KvLQT1, maybe allowing the density of KvLQT1 at the membrane surface to increase, thus increasing I_{Ks}, while hERG remains below the surface of the membrane.

Limitations of the FRET methodology must be considered when interpreting these results. Resolution is limited, so we do not know if the population of proteins we are looking at in a single ROI when performing apFRET experiments is actually located in the cell membrane. It is possible that that some of the proteins that are measured in our FRET experiments are actually located right below the surface of the membrane, maybe acting as the "reserve pool" necessary under certain physiological conditions. However, if this were the case and our results were based off of these proteins, then the functional relevance of our data is limited because these proteins are not functional, or letting through current, when they are not in the plasma membrane. One way to address this would be ideally to perform electrophysiology experiments in tandem with the FRET experiments. If changes in I_{Kr} and I_{Ks} currents after elevated intracellular cAMP levels are measurable, at least we can be sure that some of the FRET occurred between hERG and KvLQT1 at the membrane. Changes in these currents would be functional evidence that the abrogation of hERG-KvLQT1 interactions can "rescue" the mutual downregulation of

I_{Kr} and I_{Ks} observed in the transgenic rabbit models of LQTS thought to be due to the direct interactions (Brunner et al., 2008). The Darling lab is currently collaborating with the Cameron lab, which is addressing these questions with electrophysiology. However, maybe more urgently, it may be worthwhile to perform these series of experiments again using a different CNBhD of hERG that does not display any of the trafficking issues observed in the V822M mutant because the current results are inconclusive. This is currently being executed with the R823Q hERG mutant by other members of the Darling lab.

The significance of this pathway regulating hERG-KvLQT1 interactions has not yet been well characterized. It could be that cAMP-dependent phosphorylation of hERG located right below the surface of the membrane causes the conformational change necessary to dissociate hERG from KvLQT1 in response to β-adrenergic stimulation and trigger the delivery of KvLQT1 channels to the plasma membrane where they can be functional, thus adding to the growing I_{Ks} current under sympathetic stimulation. This response would then lead to increased I_{Ks} and shorter APDs, thus promoting a faster heartbeat to address the cause of the stimulation. If the interactions are indeed occurring at the surface of the cell, it is possible that phosphorylation of hERG causes the necessary conformational change to dissociate hERG from KvLQT1 while also allowing the changes in channel gating and function to occur, thus resulting in decreased hERG activation and I_{Kr} current density, as observed by Thomas et al. (1999) and Cui et al. (2000). Maybe the dissociation of hERG from KvLQT1 then promotes the necessary functional changes in KvLQT1 to allow for increased I_{Ks} in response to adrenergic stimulation.

While I have focused mainly on hERG, it may also be worthwhile to consider modifications of KvLQT1 as potentially regulating hERG-KvLQT1 interactions. The S27 KCNQ1 phosphorylation site has already been identified and the effects of cAMP-dependent phosphorylation of the N-terminus of KvLQT1 by PKA have been generally well-established (Barhanin et al., 1996; Kurokawa et al., 2003). Therefore, it would be of interest to consider the role of KvLQT1 phosphorylation in the modulation of the direct interactions between hERG and KvLQT1.

In order to address the new hypothesis that direct hERG-KvLQT1 interactions are modulated by cAMP-dependent PKA phosphorylation of either hERG or KvLQT1, or both, the same series of experiments performed in this study can be performed with phosphonull and phosphomimetic mutants of hERG and KvLQT1. Currently, the Darling lab has created a number of hERG phosphorylation mutations based on the phosphorylation sites on hERG that have been identified by Cui et al. (2001). The phosphonull mutants, where a serine or threonine has been substituted with alanine, prevents the phosphorylation of these particular amino acid sites. Phosphonull mutants of KvLQT1 are also being created to address the new hypothesis. With these mutants, then, we can determine if there are any significant changes in the interactions between hERG and KvLQT1. Ultimately, we can also determine if there are any functional changes in either of the proteins as a result of the inability of hERG and/or KvLQT1 to be phosphorylated. The phosphomimetic mutants of hERG and KvLQT1, where a serine or threonine has been substituted with an aspartate or glutamate, essentially mimics the phosphorylation state even in the absence of elevated cAMP levels. Therefore, with these mutants, we can determine if there are any differences between hERG-KvLQT1

interactions before and after elevating intracellular cAMP levels in these series of experiments.

In the case of the phosphonull mutants, we would not expect to see a significant difference in FRET efficiencies before and after increasing intracellular cAMP levels if hERG-KvLQT1 interactions are regulated by PKA phosphorylation of hERG and/or KvLQT1. FRET efficiencies should remain the same because phosphorylation of hERG and KvLQT1 at these particular sites would no longer occur, and thus the interactions would remain the same. In the case of the phosphomimetic mutants, we would not expect, again, to see a significant difference in FRET efficiencies before and after increasing intracellular cAMP levels because the phosphorylation sites of hERG and KvLQT1 in the mutants would structurally appear phosphorylated. If either of these comparisons were significantly different from one another, then that would suggest that cAMP is involved in a separate mechanism from the PKA-pathway that is responsible for modulating the hERG-KvLQT1 interactions. Ultimately, we would want to compare the FRET efficiencies between the phosphonull and -mimetic mutants in the elevated or baseline cAMP level state and demonstrate that they are significantly different from one another. More specifically, we would expect that the FRET efficiency of the phosphomimetic mutants would be significantly lower than that of the phosphonull mutants because we hypothesize that hERG and KvLQT1 would be always be interacting in the null mutants, while the interactions would be decreased in the mimetic mutants. This would then suggest that the activation of PKA by cAMP and PKA phosphorylation of hERG and/or KvLQT1 is involved in abrogating these interactions.

Overall, understanding the underlying molecular mechanism responsible for modulating the interactions between hERG and KvLQT1 could ultimately provide insight into the manifestation of LQT syndrome and other cardiac disorders and arrhythmias as well as the molecular mechanisms that shorten the APD in times of elevated heart rate in normal physiology, such as sympathetic surge. Mutations in the CNBhD of hERG have been identified that are associated with LQT2, including the V822M mutation (Splawski et al., 2000). Some of these mutations have been shown to disrupt protein trafficking and channel properties (Cui et al., 2001). Mutations have also been characterized in KCNQ1 that are associated with LQT1. The interplay between hERG and KvLQT1 is especially important during times of stress or exercise, when I_{Ks} increases as a response to an increase in sympathetic tone, to maintain regulated cardiac repolarization (Bilicski et al., 2009). Therefore, disruptions in proper hERG or KvLQT1 function can cause detrimental effects. There is evidence demonstrating hERG-KvLQT1 interactions in disease states. Most notably, the transgenic rabbit models of LQTS utilized by Brunner et al. (2008) demonstrated the presence of a functional, mutual downregulation of I_{Kr} and I_{Ks}. Bilicski et al. (2009) also demonstrated that a mutation in KCNQ1 associated with LQT1 decreased membrane localization of hERG, completely eliminating the "repolarization reserve." Determining the exact mechanism by which cAMP may play a role in hERG-KvLQT1 interactions may then provide insight into the cause of these phenomena. Thus, ultimately, elucidating the mechanism of hERG-KvLQT1 interactions at the molecular level may help to better characterize therapeutic targets and clinical intervention for LQTS and other cardiac conditions involving irregularities in action potential repolarization.

References

Abbott GW, Sesti F, Splawski I, Buck ME, Lehmann MH, Timothy KW, Keating MT, Goldistein SA. MiRP1 forms I_{Kr} potassium channels with HERG and is associated with cardiac arrhythmia. *Cell* 97: 175-187, 1999.

Akhavan A, Atanasiu R, Noguchi T, Han W, Holder N, Shrier A. Identification of the cyclic-nucleotide-binding domain as a conserved determinant of ion-channel cell-surface localization. *J Cell Science* 118: 2803-2812, 2005.

Barhanin J, Lesage F, Guillemare E, Fink M, Lazdunski M, Romey G. KvLQT1 and IsK (minK) proteins associate to form the I_{Ks} cardiac potassium current. *Nature* 384: 78-80, 1996.

Beeler GW, Reuter H. Reconstruction of the action potential of ventricular myocardial fibres. *J Physiol* 268(1): 177-210, 1977.

Benovic JL, Strasser RH, Caron MG, Lefkowitz RJ. Beta-adrenergic receptor kinase: identification of a novel protein kinase that phosphorylates the agonist-occupied form of the receptor. *Proc Natl Acad Sci USA* 83(9): 2797-2801, 1986.

Biliczki P, Virag L, Iost N, Papp JG, Varro A. Interaction of different potassium channels in cardiac repolarization in dog ventricular preparations: role of repolarization reserve. *British J Pharmacol* 137: 361-38, 2002.

Biliczki P, Girmatsion Z, Brandes RP, Harenkamp S, Pitard B, Charpentier F, Hebert TE, Hohnloser SH, Baro I, Nattel S, Ehrlich JR. Trafficking-deficient long QT syndrome mutation KCNQ1-T587M confers sever clinical phenotype by impairment of KCNH2 membrane localization: evidence for clinically significant I_{Kr}-I_{Ks} alpha-subunit interaction. *Heart Rhythm* 6: 1792-1801, 2009.

Brelidze, T. I., Carlson, A. E., Zegotta, W. N. Absence of direct cyclic nucleotide modulation of mEAG1 and hERG1 membane localizations with fluorescence and electrophysiological methods. *J Biol Chem* 284(41): 1792-1801, 2009.

Brelidze, T. I., Carlson, A. E., Sankaran, B. Zagotta, W. N. Structure of the carboxy-terminal region of a KCNH channel. *Nature* 481(7382): 530-533, 2012.

Bruggemann A, Pardo L, Stuhmer W, Pongs O. *Ether-a-go-go* encodes a voltage-gated channel permeable to K+ and Ca2+ and modulated by cAMP. *Nature* 365: 445-448, 1993.

Brunner M, Peng X, Liu GX, Ren XQ, Ziv O, Choi BR, Mathur R, Hajjiri M, Odening KE, Steinberg E, Folco EJ, Pringa E, Centracchio J, Macharzina RR, Donahay T, Schofield L, Rana N, Kirk M, Mitchell GF, Poppas A, Zehender M, Koren G.

Mechanisms of cardiac arrhythmias and sudden cardiac death in transgenic rabbits with long QT syndrome. *J Clin Invest* 118: 2246-2259, 2008.

Chen J, Stroubek J, Krishnan Y, Li Y, Bian J, McDonald TV. PKA phosphorylation of HERG protein regulates the rate of channel synthesis. *Am J Physiol Heart Circ Physiol* 296: H1244-H1254, 2009.

Cheng J, Kodama I. Two components of delayed rectifier K^+ current in heart: molecular basis, functional diversity, and contribution to repolarization. *Acta Pharmacol Sin* 25(2): 137-145, 2004.

Clancy CE, Kass RS. Inherited and acquired vulnerability to ventricular arrhythmias: cardiac Na+ and K+ channels. American Physiological Society 2005;85:33-47.

Cui J, Melman Y, Palma E, Fishman GI, McDonald TV. Cyclic AMP regulates the HERG K^+ channel by dual pathways. *Curr Biol* 10: 671-674, 2000.

Cui J, Kagan A, Qin D, Mathew J, Melman YF, McDonald TV. Analysis of the cyclic nucleotide binding domain of the HERG potassium channel and interactions with KCNE2. *J Biol Chem* 276: 17244-17251, 2001.

Ehrlich JR, Pourrier M, Weerapura M, Ethier N, Marmabachi AM, Hebert TE, Nattel S. KvLQT1 modulates the distribution and biophysical properties of HERG. A novel alpha-subunit interaction between delayed rectifier currents. *J Biol Chem* 279: 1233-1241, 2004.

Fimia GM, Sassone-Corsi P. Cyclic AMP signaling. *J Cell Sci* 114: 1971-1972, 2001.
Grant AO. Basic science for the clinical electrophysiologist: cardiac ion channels. *Circ Arrhythm Electrophysiol* 2: 185-94, 2009.

Haitin Y, Carlson AE, Zagotta WN. The structural mechanism of KCNH-channel regulation by the eag domain. *Nature* 501: 444-449, 2013.

Jespersen T, Grunnet M, Olesen SP. The KCNQ1 potassium channel: from gene to physiological function. *Physiology* 20: 408-416, 2005.

Kiehn J. Regulation of the cardiac repolarizing HERG potassium channel by protein kinase A. *Trends Cardio Med* 10(5): 205-209, 2000.

Kurokawa J, Chen L, Kass RS. Requirement of subunit expression for cAMP-mediated regulation of a heart potassium channel. *Proc Natl Acad Sci USA* 100: 2122-2127, 2003.

Li Q, Ng HQ, Yoon HS, Kang C. Insight into the molecular interaction between the cyclic nucleotide-binding homology domain and the eag domain of the hERG channel. *FEBS Lett* 588(17): 2782-2788, 2014.

Marque-Carvalho MJ, Sahoo N, Muskett FW, Vieira-Pires RS, Gabant G, Cadene M, Schonherr R, Morais-Cabral JH. Structural, biochemical, and functional characterization of the cyclic nucleotide binding homology domain for the mouse EAG1 potassium channel. *J Mol Biol* 423: 34-46, 2012.

Marx SO, Kurokawa J, Reiken S, Motoike H, D'Armiento J, Marks AR, Kass RS. Requirement of a macromolecular signaling complex for β adrenergic receptor modulation of the KCNQ1-KCNE1 potassium channel. *Science* 295: 496-499, 2002.

Nicholas C, Park KH, Harchi AE, Camonis J, Kass RS, Escande D, Merot J, Loussouarn G, Le Bouffant F, Baro I. I_{Ks} response to protein kinase A-dependent KCNQ1 phosphorylation requires direct interaction with microtubules. *Cardiovas Res* 79: 427-435, 2008.

Organ-Darling LE, Vernon AN, Giovanniello JR, Lu Y, Moshal K, Roder K, Li W, Koren G. Interactions between hERG and KCNQ1 α-subunits are mediated by their COOH termini and modulated by cAMP. *Am J Physiol Heart Circ Physiol* 304: H589-h599, 2013.

Ren XQ, Liu GX, Organ-Darling LE, Zheng R, Roder K, Jindal HK, Centracchio J, McDonald TV, Koren G. Pore mutants of HERG and KvLQT1 downregulate the reciprocal currents in stable cell lines. *Am J Physiol Heart Circ Physiol* 299: H1525-H1534, 2010.

Roden DM. Repolarization reserve. A moving target. *Circulation* 118: 981-982, 2008.

Sanguinetti MC, Curran ME, Zou A, Shen J, Spector PS, Atkinson DL, Keating MT. Coassembly of KvLQT1 and minK (IsK) proteins to form cardiac I_{Ks} potassium channel. *Nature* 384: 80-83, 1996.

Sanguinetti MC, Tristani-Firouzi M. hERG potassium channels and cardiac arrhythmia. *Nature* 440: 463-469, 2006.

Satler CA, Walsh EP, Vesely MR, Plummer MH, Ginsburg GS, Jacob HJ. Novel missense mutation in cyclic nucleotide-binding domain of *HERG* causes long QT syndrome. *Am J Med Genet* 65: 27-35, 1996.

Sun Y, Rombola C, Jyothikumar V, Periasamy A. Forster resonance energy transfer microscopy and spectroscopy for localizing protein-protein interactions in living cells. *Cytometry A* 83(9): 780-793, 2013.

Thomas D, Zhang W, Karle CA, Kathofer S, Schols W, Kubler W, Kiehn J. Deletion of protein kinase A phosphorylation sites in the HERG potassium channel inhibits activation shift by protein kinase A. *J Biol Chem* 274: 27457-27462, 1999.

Vandenberg JI, Perry MD, Perrin MJ, Mann SA, Ke Y, Hill AP. hERG K+ channels: structure, function, and clinical significance. *Physiol Rev* 92: 1393-1478, 2012.

Warmke JW, Ganetzky B. A family of potassium channel genes related to *eag* in *Drosophila* and mammals. *Proc Natl Acad Sci USA* 91: 3438-3442, 1994.

Weerapura M, Nattel S, Chartier D, Caballero R, Hébert TE. A comparison of currents carried by HERG, with and without coexpression of MiRP1, and the native rapid delayed rectifier current. Is MiRP1 the missing link? *J Physiol* 540(1): 15-27, 2002.